

Supporting Information for

Dual responsive pyridoxal-AHMT based fluorescent sensor towards zinc(II) and mercury(II) ions and its bioimaging application

Kettalu Ananthan Karthick^a, Bhaskaran Shankar^b, Santhalingam Gayathri^c, Manikka Kubendran
Aravind^c, Balasubramaniam Ashokkumar^c, Arunachalam Tamilselvi^{*a}

^a*PG & Research Department of Chemistry, Thiagarajar College (Affiliated to Madurai Kamaraj
University), Madurai 625 009, India*

^b*Department of Chemistry, Thiagarajar College of Engineering, Madurai 625 015, India*

^c*School of Biotechnology, Madurai Kamaraj University, Madurai 625 021, Tamil Nadu, India*

*Email: tamilselvi_chem@tcarts.in

S. No.	Figures and tables Content	Page No.
1.	Materials and Methods, Details of Solid state diffuse reflectance (UV-DRS) study, Solid state emission study, Job plot analysis, Quantum yield determination, Photoluminescence lifetime measurements, Hirshfeld surface analysis, MTT assay, and Benesi-Hildebrand (B-H) method	S5-S8
2.	Fig. S1. UV-Vis spectrum of probe, L (50 μM) in HEPES buffered (pH = 8.0) (DMSO:water (1:1, v/v)).	S9
3.	Fig. S2. Emission spectrum of probe, L (50 μM) in HEPES buffered (pH = 8.0) (DMSO:water (1:1, v/v)); $\lambda_{\text{ex}} = 336 \text{ nm}$.	
4.	Fig. S3. FT-IR spectra of (a) L (b) L + Zn²⁺ and (c) L + Hg²⁺ .	S10
5.	Fig. S4. ¹ H NMR spectrum of probe, L (DMSO- <i>d</i> 6, 400 MHz).	
6.	Fig. S5. ¹³ C NMR spectrum of probe, L (DMSO- <i>d</i> 6, 100 MHz).	S11
7.	Fig. S6. Q-TOF HRMS spectrum of probe, L .	
8.	Fig. S7. Stick model of L showed the intra and intermolecular H-bond distance.	S12
9.	Fig. S8. TGA/DTA plots of (a) L (b) ZnL₂ and (c) Hg₂L₂ .	
10.	Fig. S9. Crystal packing view of L showing the existence of aromatic π - π interactions in the crystal (lattice water molecules and hydrogens are omitted for clarity).	S13
11.	Fig. S10. Comparison of powder XRD pattern of experimental with simulated pattern (generated from CIF file using Mercury 3.0 software package).	
12.	Fig. S11. Selective absorbance response of L (50 μM) in HEPES buffered (pH = 8.0) (DMSO:water (1:1, v/v)) towards competitive metal ions.	S14
13.	Fig. S12. Fluorescence spectra of L (50 μM) in various solvents; $\lambda_{\text{ex}} = 336 \text{ nm}$.	
14.	Fig. S13. Effect of pH on the fluorescence intensity of probe, L (50 μM).	S15
15.	Fig. S14. Effect of pH on the fluorescence intensity of probe, L (50 μM) in the absence and presence of Zn²⁺ (25 μM).	
16.	Fig. S15. Effect of pH on the fluorescence intensity of probe, L (50 μM) in the absence and presence of Hg²⁺ (50 μM).	S16
17.	Fig. S16. Fluorescence spectra of L (50 μM) in various ratios (v/v) of DMSO and water in HEPES buffered medium (pH = 8.0).	
18.	Fig. S17. Normalised excitation and emission spectra of probe, L ($\lambda_{\text{ex}} = 309, 336 \text{ and } 398 \text{ nm}$).	S17
19.	Fig. S18. UV-Vis titration of L (50 μM) in HEPES buffered (pH = 8.0) (DMSO:water (1:1, v/v)) medium upon addition of Zn²⁺ ; gradually increasing [Zn²⁺] from 0 to 25 μM , excess addition till 35 μM . Inset: The plot of absorbance intensity at 405 and 336 nm versus concentration of Zn²⁺ .	
20.	Fig. S19. UV-Vis titration of L (50 μM) in HEPES buffered (pH = 8.0) (DMSO:water (1:1, v/v)) medium upon addition of Hg²⁺ ; gradually increasing [Hg²⁺] from 0 to 50 μM , and excess addition till 60 μM . Inset: The plot of absorbance intensity at 388 and 336 nm versus concentration of Hg²⁺ .	S18
21.	Fig. S20. Illustration of keto-enol tautomerism <i>via</i> six-membered transition state.	
22.	Fig. S21. Benesi-Hildebrand (B-H) plot of fluorescence changes at 440 nm upon addition of Zn²⁺ ion (linearity plotted using the addition from 10 μM to 25 μM of Zn²⁺ to L).	S19
23.	Fig. S22. Benesi-Hildebrand (B-H) plot of fluorescence changes at 478 nm upon addition of Hg²⁺ ion (linearity plotted using the addition from 10 μM to 50 μM of Hg²⁺ to L).	

24.	Fig. S23. Stern-Volmer plot of fluorescence changes at 478 nm upon addition of Hg^{2+} ion (linearity plotted using the addition from 25 μM to 50 μM of Hg^{2+} to L).	S20
25.	Fig. S24. Job's plot for (a) ZnL_2 and (b) Hg_2L_2 formation using emission spectral data of ($\lambda_{\text{ex}} = 336 \text{ nm}$).	
26.	Fig. S25. Determination of LOD (a) Linear regressive plot of L with Zn^{2+} ion concentration from 5 to 25 μM (b) Linear regressive plot of L with Hg^{2+} ion concentration from 5 to 50 μM .	S21
27.	Fig. S26. (a) Time course measurement study of L (60 μM) in the presence and absence of Zn^{2+} and Hg^{2+} (60 μM); The full spectrum viewed and labeled as (b), (c) and (d) are 3D plot of interval scan measurements of L , L + Zn^{2+} and L + Hg^{2+} in HEPES buffered (pH = 8.0) (DMSO:water (1:1, v/v)) medium	S22
28.	Fig. S27. Fluorescence Interference study of L in the presence of competitive metal ions (1 equiv.) with and without Zn^{2+} ion (1.0 equiv.) HEPES buffered (pH = 8.0) (DMSO:water (1:1, v/v)).	
29.	Fig. S28. Fluorescence Interference study of L in the presence of competitive metal ions (1 equiv.) with and without Hg^{2+} ion (1 equiv.) HEPES buffered (pH = 8.0) (DMSO:water (1:1, v/v)).	S23
30.	Fig. S29. Fluorescence spectra recorded in HEPES buffered (pH = 8.0) (DMSO:water (1:1, v/v)) medium; (a) Reversibility of L + Zn^{2+} with EDTA (b) Reversibility of L + Hg^{2+} with EDTA.	
31.	Fig. S30. Recovery cycles of (a) L (50 μM) upon alternative addition of Zn^{2+} (1 equiv.) and EDTA (1 equiv.); (b) L (50 μM) upon alternative addition of Zn^{2+} (1 equiv.) and EDTA (1 equiv.)	
32.	Fig. S31. Partial ^1H NMR spectral titration of probe with successive addition of $\text{Zn}(\text{OAc})_2$ in DMSO- <i>d</i> ₆ for zoomed view of aromatic –OH and exocyclic –NH signal changes.	S24
33.	Fig. S32. Partial ^1H NMR spectral titration of probe with successive addition of $\text{Zn}(\text{OAc})_2$ in DMSO- <i>d</i> ₆ for zoomed view of endocyclic –NH signal changes.	
34.	Fig. S33. Partial ^1H NMR spectral titration of probe with successive addition of $\text{Zn}(\text{OAc})_2$ in DMSO- <i>d</i> ₆ for zoomed view of azomethine signal changes.	S25
35.	Fig. S34. Partial ^1H NMR spectral titration of probe with successive addition of $\text{Zn}(\text{OAc})_2$ in DMSO- <i>d</i> ₆ for zoomed view of aliphatic –OH and –NH ₂ signal changes.	
36.	Fig. S35. Partial ^1H NMR spectral titration of probe with successive addition of HgCl_2 in DMSO- <i>d</i> ₆ for zoomed view of endocyclic –NH signal changes.	S26
37.	Fig. S36. Partial ^1H NMR spectral titration of probe with successive addition of HgCl_2 in DMSO- <i>d</i> ₆ for zoomed view of exocyclic –NH and Ar-OH signal changes.	
38.	Fig. S37. ^{13}C NMR spectra of probe (L) with 1.0 equivalent addition of HgCl_2 in DMSO- <i>d</i> ₆ (100 MHz) Note; the asterisk symbol * indicated that trace amount of methanol solvent.	S27
39.	Fig. S38. Possible tautomeric forms of probe (L).	
40.	Fig. S39. Frontier molecular orbital diagram of L , ZnL_2 and Hg_2L_2 in gas phase level.	S28
41.	Fig. S40. Frontier molecular orbital diagram of L , ZnL_2 and Hg_2L_2 in water medium.	
42.	Fig. S41. Frontier molecular orbital diagram of L , ZnL_2 and Hg_2L_2 in DMSO medium.	
43.	Fig. S42. Calculated UV-Vis spectra (red) with oscillator strengths (blue) of (a) L in water medium (b) L in DMSO medium (c) ZnL_2 in water medium (d) ZnL_2 in DMSO medium (e) Hg_2L_2 in water medium and (f) Hg_2L_2 in DMSO medium; The black colour represents the experimental UV-Vis results.	S29

44.	Fig. S43. Solid state UV-DRS spectra of L , L + Zn(II) and L + Hg(II) , Inset: Kubelka–Munk (K–M) plot used for band gap calculations.	S30
45.	Fig. S44. Hirshfeld surfaces mapped over (a) d_i ; (b) d_e ; (c) d_{norm} ; (d) shape index; and (e) curvedness for probe (L).	S31
46.	Fig. S45. Two-dimensional fingerprint (2D) plots of probe (L) generated from Crystal Explore software.	
47.	Fig. S46. Determination of cytotoxicity of L on A549 cells by MTT assay.	S32
48.	Fig. S47. Comparison plot of normalized absorbance and emission spectra of L , L + Zn²⁺ and L + Hg²⁺ (Stokes shift analysis).	
49.	Table S1. FT-IR assignments of L , L + Zn²⁺ and L + Hg²⁺ .	S33&S34
50.	Table S2. Crystal data and structure refinement for L .	
51.	Table S3. Bond lengths [Å] and angles [°] for L .	S34-S36
52.	Table S4. Summarized λ_{max} (nm) emission data of L in various solvents.	S37
53.	Table S5. Summarized λ_{max} (nm) emission data of L in various ratios (v/v) of DMSO and water in HEPES buffered medium (pH = 8.0).	
54.	Table S6. Solid and solution state fluorescence lifetime data of L , ZnL₂ and Hg₂L₂	
55.	Table S7. The Cartesian coordinates of L (enol-thione), ZnL₂ and Hg₂L₂ calculated from Gaussian-09 at B3LYP computational level using IEF-PCM calculation (water as solvent).	S38-S41
56.	Table S8. The Cartesian coordinates of L (enol-thione), ZnL₂ and Hg₂L₂ calculated from Gaussian-09 at B3LYP computational level using IEF-PCM calculation (DMSO as solvent).	
57.	Table S9. Major UV-Vis electronic transitions and corresponding orbital contributions for L , ZnL₂ and Hg₂L₂ .	S42
58.	Table S10. Selected Frontier molecular orbitals HOMO-LUMO diagram of probe (L) in water and DMSO medium.	S43&S44
59.	Table S11. Selected Frontier molecular orbitals HOMO-LUMO diagram of zinc(II) complex (ZnL₂) in water and DMSO medium	S45-S51
60.	Table S12. Selected Frontier molecular orbitals HOMO-LUMO diagram of mercury(II) complex (Hg₂L₂) in water and DMSO medium.	
61.	Table S13. Comparison with recent literature results.	
62.	Reference	S52&S53

Materials and Methods

Pyridoxal hydrochloride, 4-amino-3-hydrazinyl-1,2,4-triazole-5-thione and chloride salt of metals (Ag^+ , Al^{3+} , Ba^{2+} , Cd^{2+} , Cu^{2+} , Co^{2+} , Fe^{3+} , Hg^{2+} , K^+ , Mn^{2+} , Mg^{2+} , Ni^{2+} , Na^+ , Pb^{2+} , Pd^{2+} , Sr^{2+} and Zn^{2+}) were procured from commercial sources and utilized for synthesis and fluorescence sensor studies. All the organic solvents and double distilled water of spectroscopic grade used for carrying out the photophysical studies. The probe was purified with silica gel column (230–400 mesh) and crystallized in binary mixtures of methanol with water. All the sensor studies were executed in HEPES buffer (pH = 8.0) (DMSO:water (1:1, v/v)) mixture. Absorbance spectral data measured on spectrophotometer (Jasco UV-730) and Solid and solution state emission spectra were collected using spectrofluorometer (Jasco FP-8300 model). The solid state UV-Vis Diffuse Reflectance spectra (DRS) were measured with a spectrophotometer (Jasco UV, Model V-770). The solid and solution state fluorescence decay analysis were performed on Horiba Jobin Yvon Fluorocube life time system. FT-IR spectral data collected on Jasco FT/IR-4700typeA spectrometer. ^1H and ^{13}C NMR spectra were recorded on a Bruker Avance Onebay 400 MHz FT-NMR spectrometer. ^1H NMR titration was performed using DMSO-*d*6 solvents by keeping total volume of 600 μL . The zinc(II) acetate and mercury(II) chloride salts were used as metal ion sources. HRMS/Q-TOF spectrometer (Agilent make; 6200 series) was utilized to collect mass spectral data. Single crystal X-ray diffraction data was collected on a Bruker D8 Quest diffractometer. Thermogravimetric (TGA/DTA) analysis was performed on NJA – STA 2500 thermal analyser Regulus instrument. The pH dependency studies were executed on Labtech digital pH meter.

Solid state diffuse reflectance (UV-DRS) study

The fine powdered samples of **L**, **L + Zn²⁺** and **L + Hg²⁺** were carefully filled with solid sample cell holder. Before measuring UV-DRS, baseline is corrected and calibrated with barium sulphate standard. The correlation between absorption co-efficient (α) and optical band gap (E_g) is given by the equation (1),

$$\alpha E \approx A_1(E - E_g)^2 \quad \dots(1)$$

Where, $E = h\nu$ is photon energy, A_1 is a constant

Kubelka–Munk (K–M)^[1] equation (2) is given by,

$$F(R) = \frac{(1 - R^2)}{2R} = \frac{k}{s} \quad \dots(2)$$

Where, R is experimentally observed reflectance, k is molar absorption co-efficient and s is scattering co-efficient. The scattering co-efficient is independent on the wavelength of incident light and using equation (1) & (2), the following equation (3) can be written as follows,

$$[h\nu F(R)]^{\frac{1}{2}} = A_1[h\nu - E_g] \quad \dots(3)$$

The plot Kubelka–Munk (K–M) function $[h\nu F(R)]^{1/2}$ versus photon energy is known as Tauc plot.^[2] The optical band gap energy (E_g) of **L**, **L + Zn²⁺** and **L + Hg²⁺** were determined by extrapolating the linear fitted region to $[h\nu F(R)]^{1/2} = 0$.

Solid state emission study

Powdered forms of **L**, **L + Zn²⁺** and **L + Hg²⁺** were carefully load on FDA-808 solid sample holding block (FP-8300 model) and fix the excitation wavelength ($\lambda_{ex} = 336$ nm) to obtain the solid state emission. Normalise the solid state fluorescence intensity of **L**, **L + Zn²⁺** and **L + Hg²⁺** for comparing the wavelength shift.

Job's plot analysis

Stock solutions of probe (**L**) and metal ions (**Zn²⁺** and **Hg²⁺**) were made (5×10^{-6} M) in HEPES buffered (pH = 8.0) (DMSO:water (1:1, v/v)) for Job's plot analysis. The emission for the molar ratio between **L** and metal ion (**Zn²⁺** and **Hg²⁺**) ranging from 0 to 0.9 were measured and plotted between molar ratio and emission intensity.^[3]

Photoluminescence quantum yield calculations

The relative standard method^[4] applied for calculating quantum yield (equation (4)).

$$\phi_s = \phi_{ref} \left(\frac{I_s}{I_{ref}} \right) \left(\frac{A_{ref}}{A_s} \right) \left(\frac{\eta_s^2}{\eta_{ref}^2} \right) \quad \dots(4)$$

Where ϕ_s and ϕ_{ref} are the quantum yields of unknown sample and the standard (quinine sulphate: $\phi_{ref} = 0.546$) respectively, I_s and I_{ref} are the area of integrated fluorescence intensities, A_s and A_{ref} are the optical density for the sample and standard, η_s and η_{ref} are the refractive indices of the solvents

Solid and solution state fluorescence lifetime measurement

Fluorescence lifetime decay measurement was carried out on Horiba Jobin Yvon M/S Fluorocube - Lifetime system, employed with time correlated single photon counting (TCSPC) experiment. The suitable excitation wavelength ($\lambda_{\text{ex}} = 336 \text{ nm}$) was studied in steady state emission, we have used pulsed-Diode Nano-LED of 340 nm as excitation signal source for both solid and solution state (HEPES buffered (pH = 8.0) (DMSO:water (1:1, v/v))) lifetime decay. The pulse repetition rate of TCSPC was set as 1 MHz. The detector response for the 340 nm light source was 1.122 and 1.117 ns for solid and solution state lifetime decay respectively. The full width-half maximum (FWHM) of the prompt is 10.0473 ch (solid) and 9.9964 ch (solution). The prompt time calibration is $1.117 \times 10^{-10} \text{ sec/ch}$ which is used to convert channels to nanoseconds. The instrument response function (IRF) was measured with a scatterer LUDOX AS40 colloidal silica medium. The fluorescence decay data fitting was analysed by IBH (DAS-6) software. A value of exponential fits (χ^2) acceptable range was further judged by the symmetrical distribution of the residuals. The three exponentials decay gives three lifetimes; we have calculated and reported average lifetime for both solid and solution state measurements.

Hirshfeld surface analysis

Hirshfeld surface analysis was used to investigate close contacts in molecular packing, intermolecular atomic interactions and its contribution percentage within the crystal structure.^[51] The surface mapping and 2D fingerprint plots (plot of d_i versus d_e) were generated from the single crystal X-ray data of probe (**L**) on Crystal Explorer 3.1 software package. The various graphical views, d_e (distance from a point of surface to the nearest nucleus outside the surface), d_i (distance from a point of surface to the nearest nucleus inside the surface), normalised d_{norm} (normalised distance), shape-index, and curvedness were generated in order to understand intermolecular interactions.

MTT assay

The cell viability of **L** was investigated using standard MTT (3-(4,5-dimethylthiazol-2-yl)-2,5-diphenyltetrazolium bromide) assay on A549 cell line. Cells were seeded in 96-well plate with an initial seeding density of 0.01×10^6 cells per well and incubated in CO₂ incubator in

DMEM media with 10% FBS for 16 h. After incubation, cells were treated with varying concentrations of **L** from 10 µg to 140 µg (33.70 to 471.80 µM) for 12 h. Following that, cells were washed twice with phosphate buffer and treated with MTT for 4 h. After which, MTT was removed and 90 µL of DMSO was added and the cells were further incubated for 15 min. A purple colour production was observed and the optical density (OD) was measured in a microtiter plate reader at 570 nm to determine IC₅₀ value, with untreated cells taken as controls.

Benesi-Hildebrand (B-H) method

The binding constant (K_b) was estimated using Benesi-Hildebrand equation^[6] based on fluorescence titration data. The inverse of the slope in linear regressive plot equals to binding constant (K_b) for Zn^{2+} complexation with probe. The mathematical expression of Benesi-Hildebrand equation (for 2:1 stoichiometric) for the fluorescence titration is shown in below equation (5),

$$\frac{F_{max}-F_0}{F-F_0} = \frac{1}{K_b[Zn^{2+}]^2} \quad \dots(5)$$

Where, F_0 is fluorescence intensity of molecular sensor in the absence of Zn^{2+} ion. F is fluorescence intensity of molecular sensor in the presence of Zn^{2+} ion. F_{max} is maximum fluorescence intensity of molecular sensor at the saturation level. The Benesi-Hildebrand equation for 1:1 stoichiometric complex is shown in equation (6),

$$\frac{1}{F-F_0} = \frac{1}{F-F_s} + \frac{1}{(K_b(F-F_0)[Hg^{2+}])} \quad \dots(6)$$

Where, F_0 is fluorescence intensity of probe in the absence of Hg^{2+} ion. F is fluorescence intensity of **L** in the presence of Hg^{2+} ion. F_s is fluorescence intensity of **L** at the saturation level. The ratio between the intercept and slope in linear regressive plot equals to binding constant (k_b)

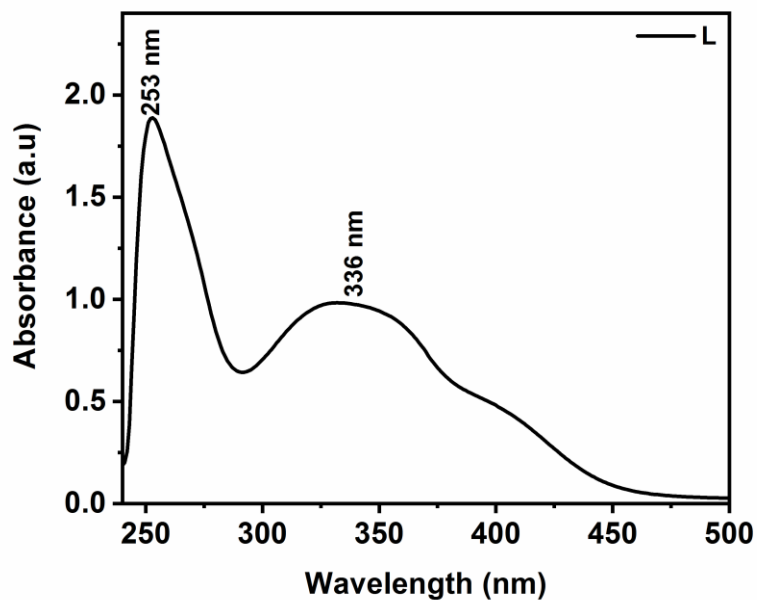


Fig. S1. UV-Vis spectrum of probe, **L** (50 μ M) in HEPES buffered (pH = 8.0) (DMSO:water (1:1, v/v)).

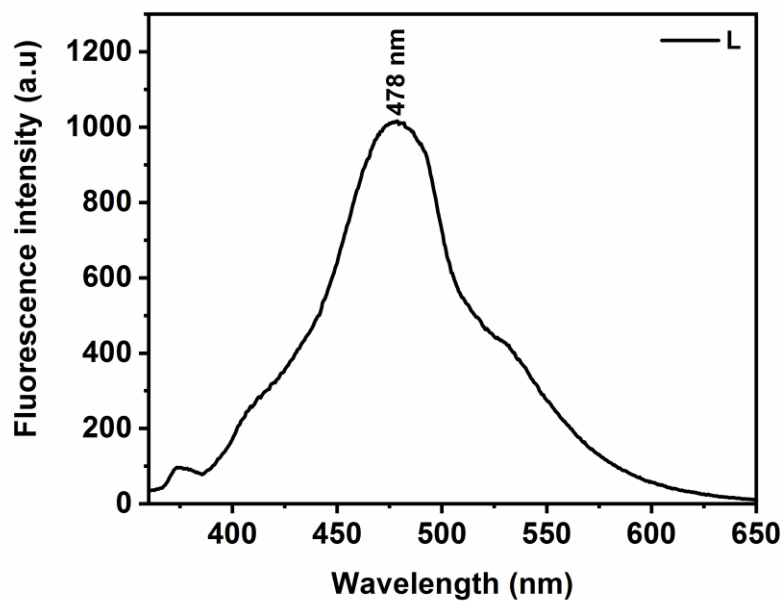


Fig. S2. Emission spectrum of probe, **L** (50 μ M) in HEPES buffered (pH = 8.0) (DMSO:water (1:1, v/v)); $\lambda_{\text{ex}} = 336$ nm.

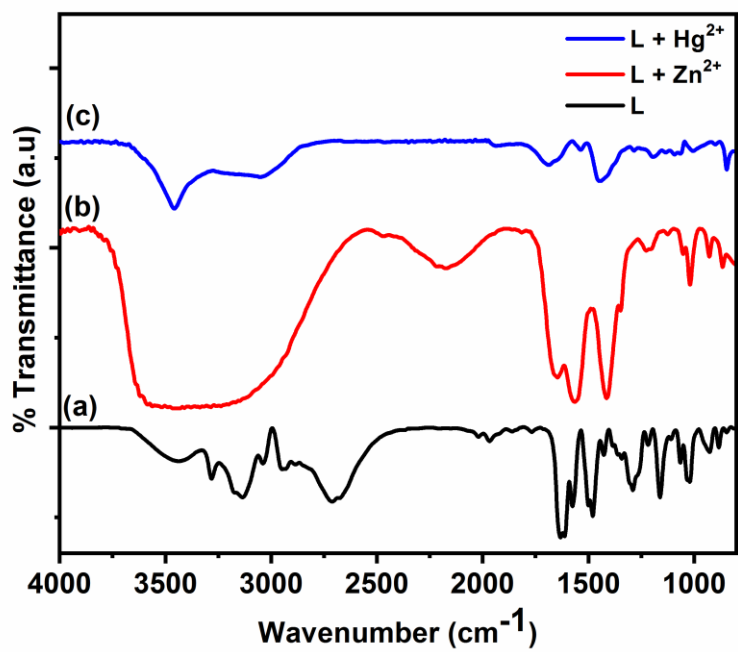


Fig. S3. FT-IR spectra of (a) L (b) L + Zn²⁺ and (c) L + Hg²⁺.

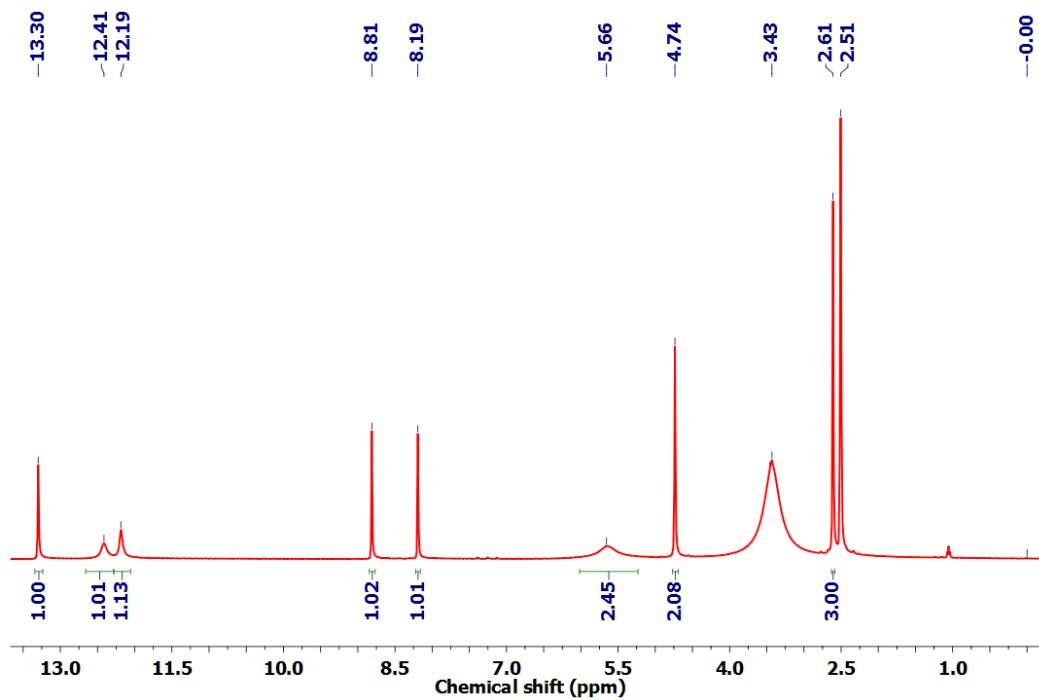


Fig. S4. ¹H NMR spectrum of probe, L (DMSO-d₆, 400 MHz).

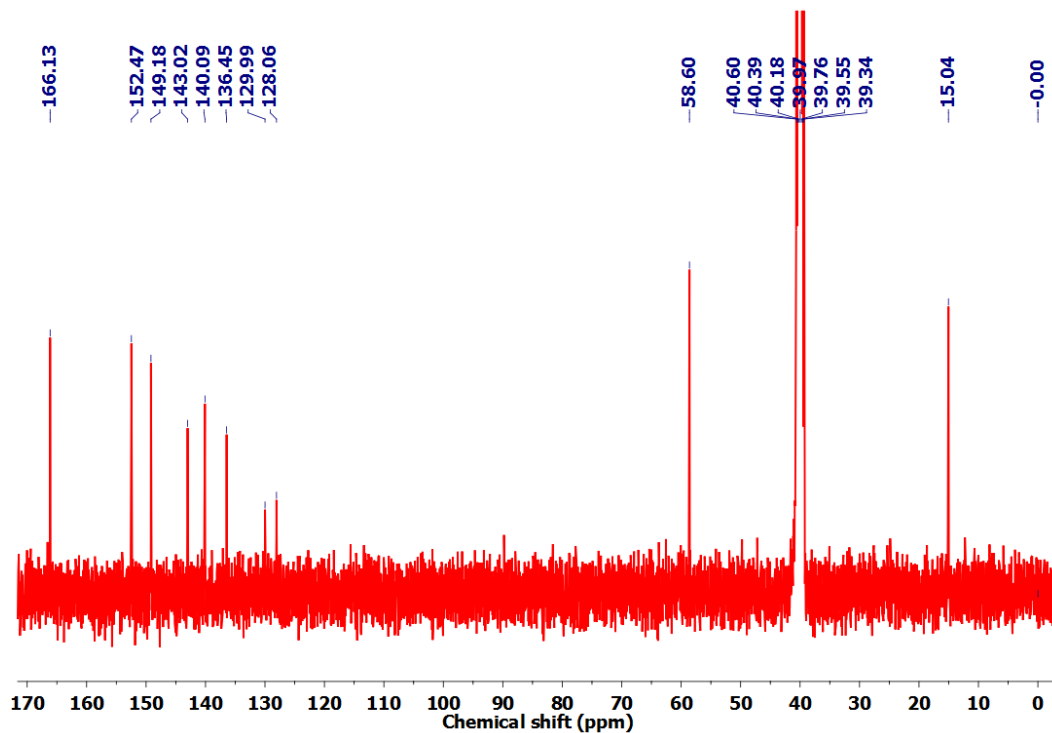
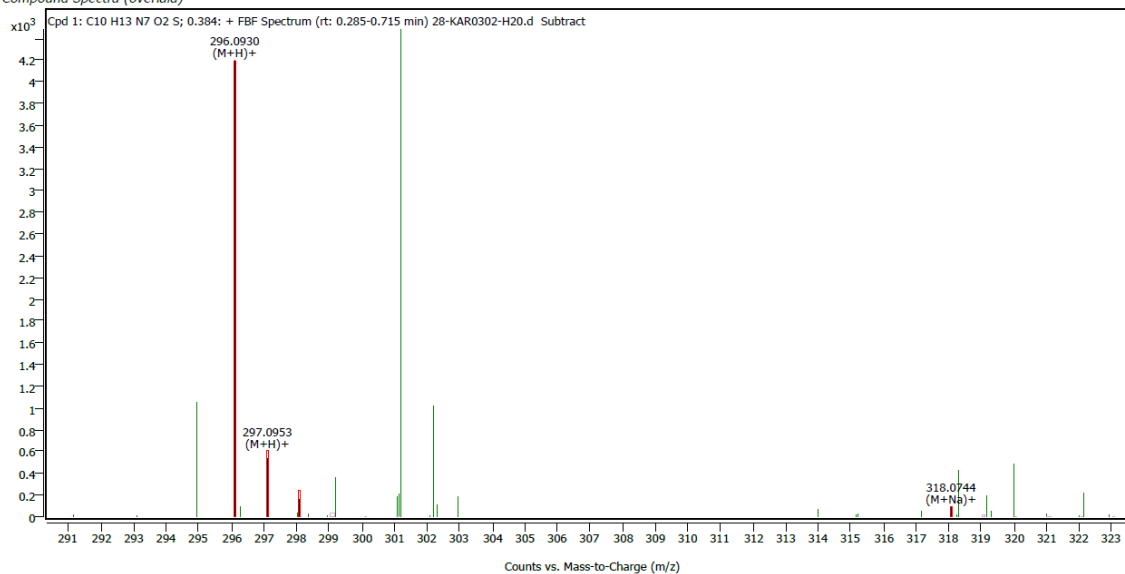


Fig. S5 ^{13}C NMR spectrum of probe, L (DMSO- d_6 , 100 MHz).

Compound Details

Cpd. 1: C₁₀ H₁₃ N₇ O₂ S

Compound Spectra (overlaid)



Compound ID Table

Cpd	Formula	Mass (Tgt)	Calc. Mass	Mass	Species	Diff(Tgt.ppm)	mDa
1	C ₁₀ H ₁₃ N ₇ O ₂ S	295.0851	295.0858	296.0930 318.0744	(M+H)+ (M+Na)+	2.07	0.61

Fig. S6. Q-TOF HRMS spectrum of probe, L.

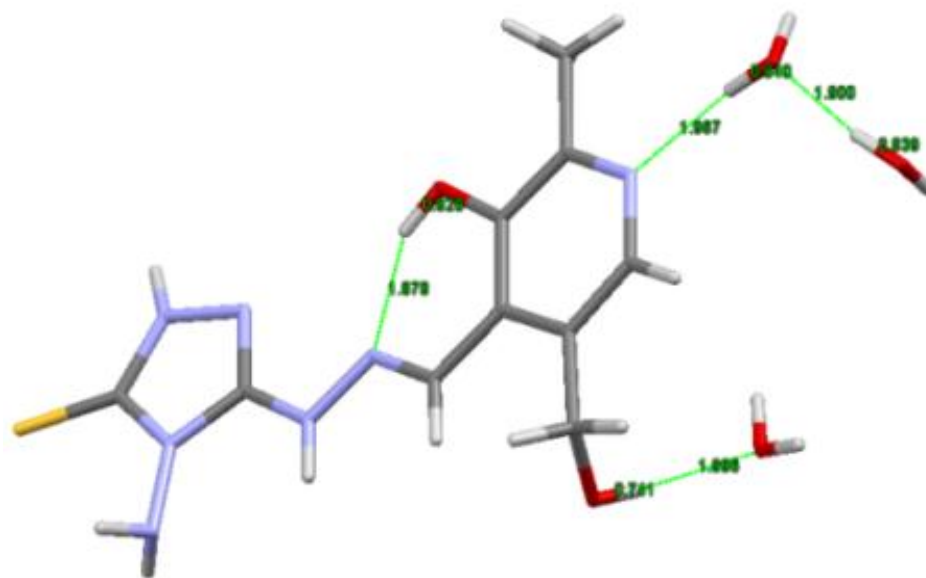


Fig. S7. Stick model of L showed the intra and intermolecular H-bond distance.

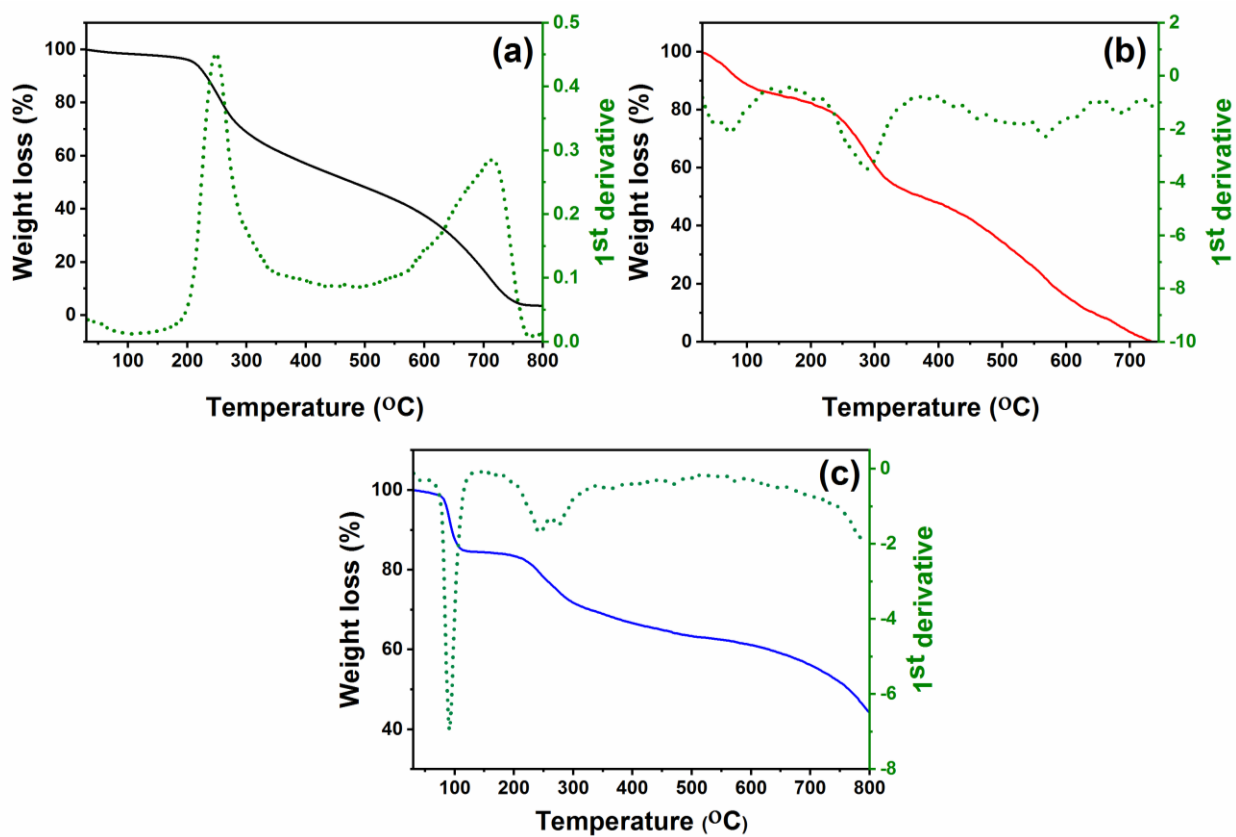


Fig. S8. TGA/DTA plots of (a) L (b) ZnL₂ and (c) Hg₂L₂.

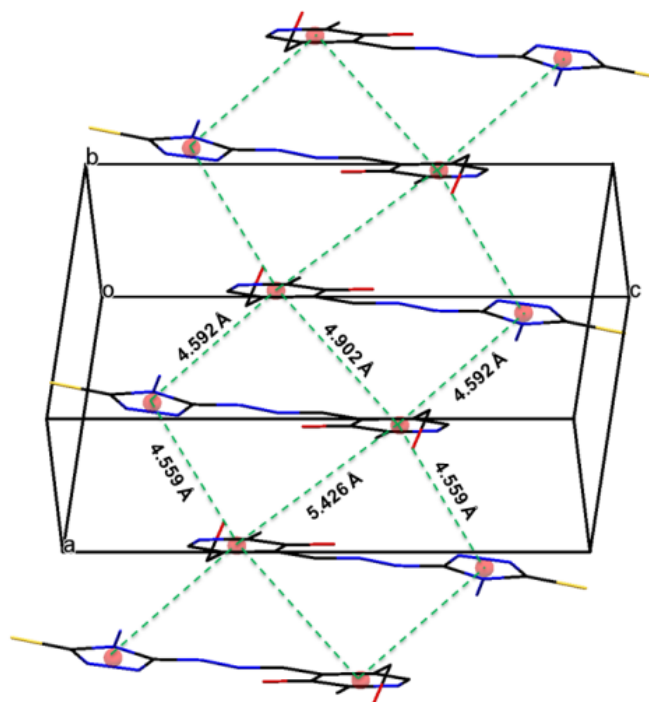


Fig. S9. Crystal packing view of **L** showing the existence of aromatic π - π interactions in the crystal (lattice water molecules and hydrogens are omitted for clarity).

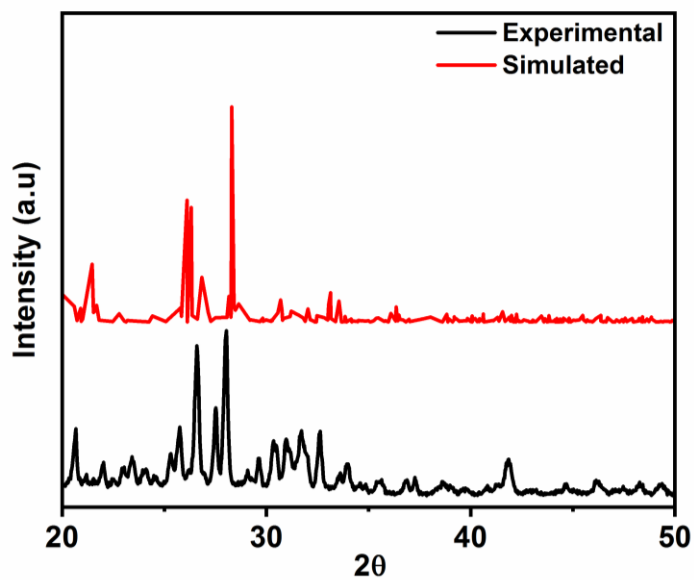


Fig. S10. Comparison of powder XRD pattern of experimental with simulated pattern (generated from CIF file using Mercury 3.0 software package).

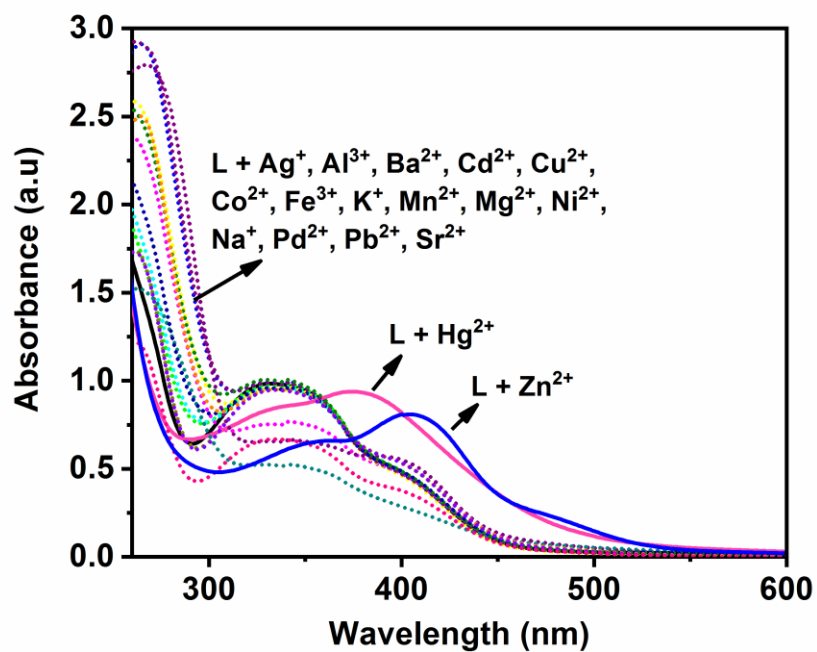


Fig. S11. Selective absorbance response of **L** (50 μM) in HEPES buffered (pH = 8.0) (DMSO:water (1:1, v/v)) towards competitive metal ions.

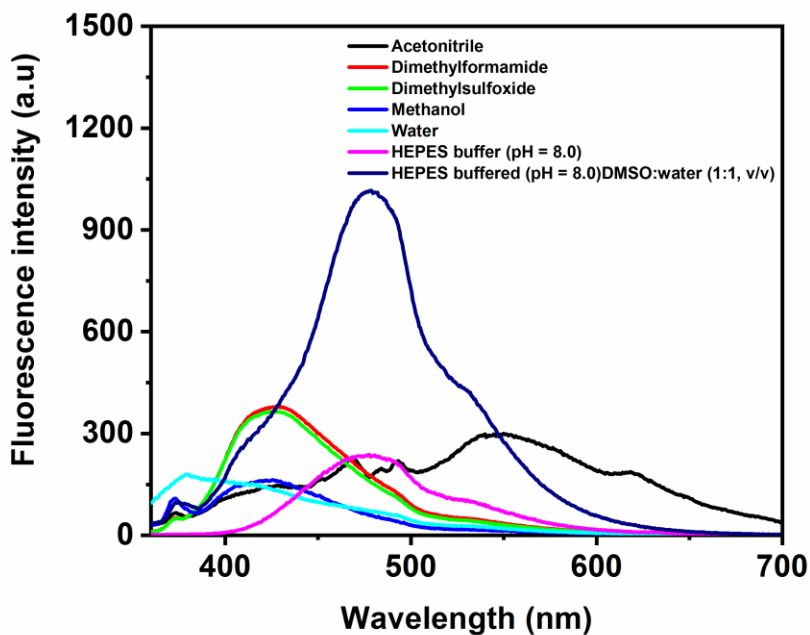


Fig. S12. Fluorescence spectra of **L** (50 μM) in various solvents; $\lambda_{\text{ex}} = 336 \text{ nm}$.

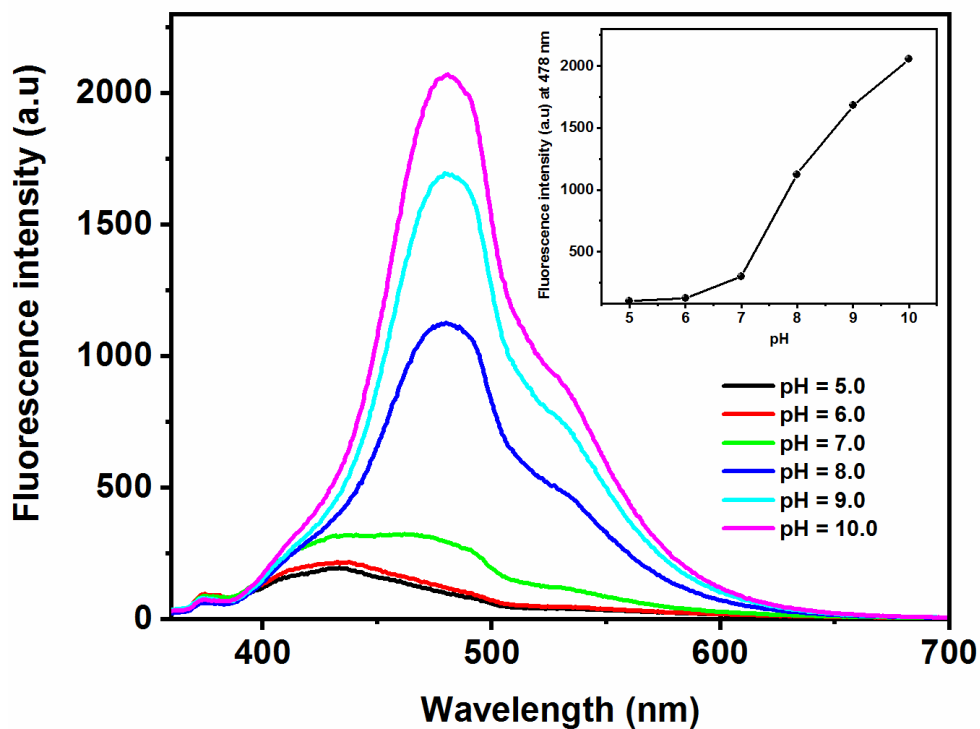


Fig. S13. Effect of pH on the fluorescence intensity of probe, **L** (50 μM).

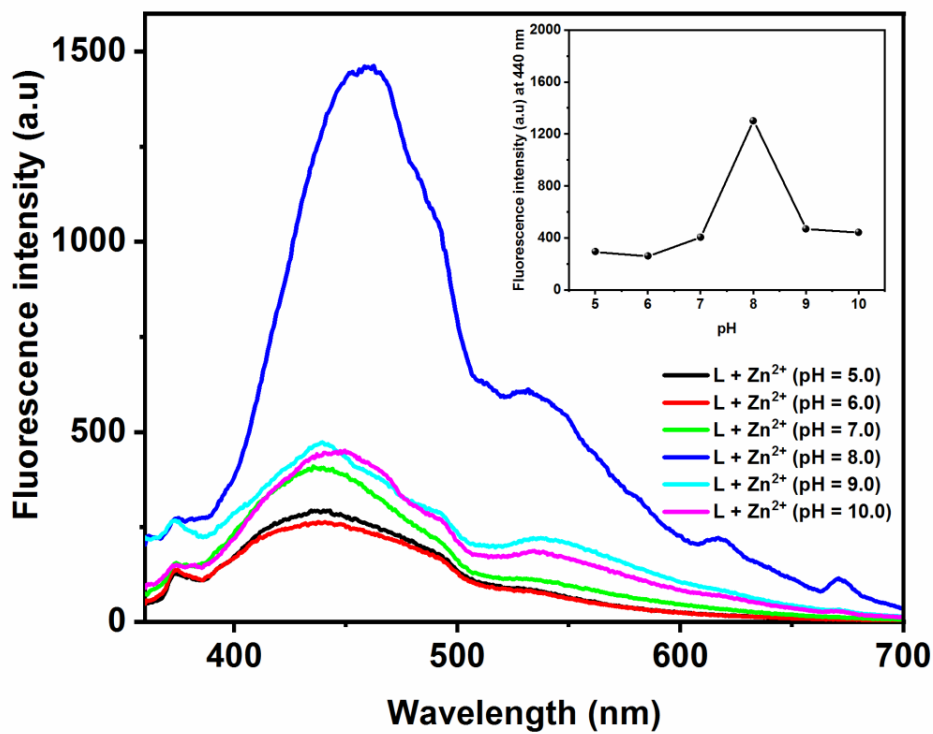


Fig. S14. Effect of pH on the fluorescence intensity of probe, **L** (50 μM) in the absence and presence of Zn²⁺ (25 μM).

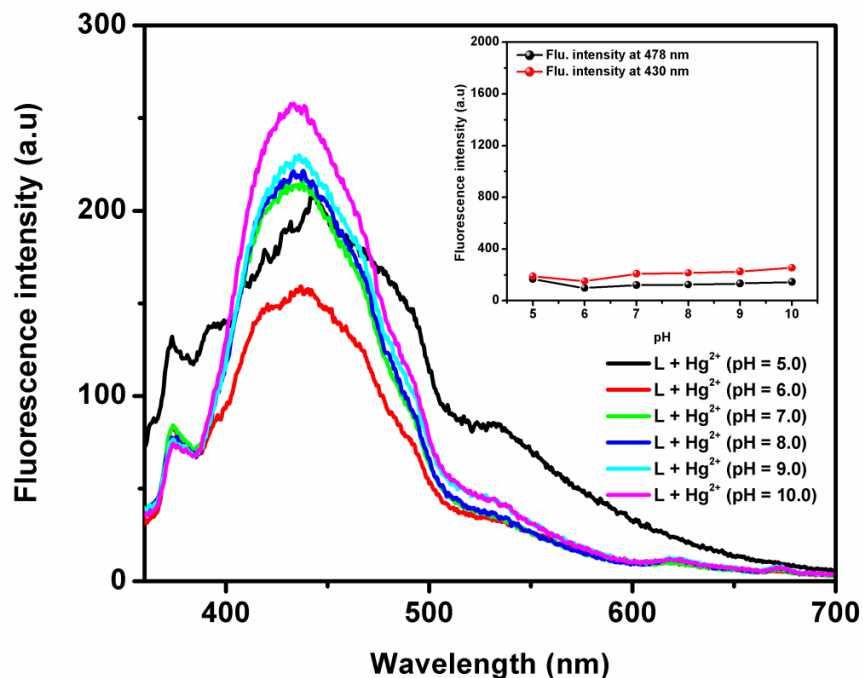


Fig. S15. Effect of pH on the fluorescence intensity of probe, L (50 μM) in the absence and presence of Hg²⁺ (50 μM).

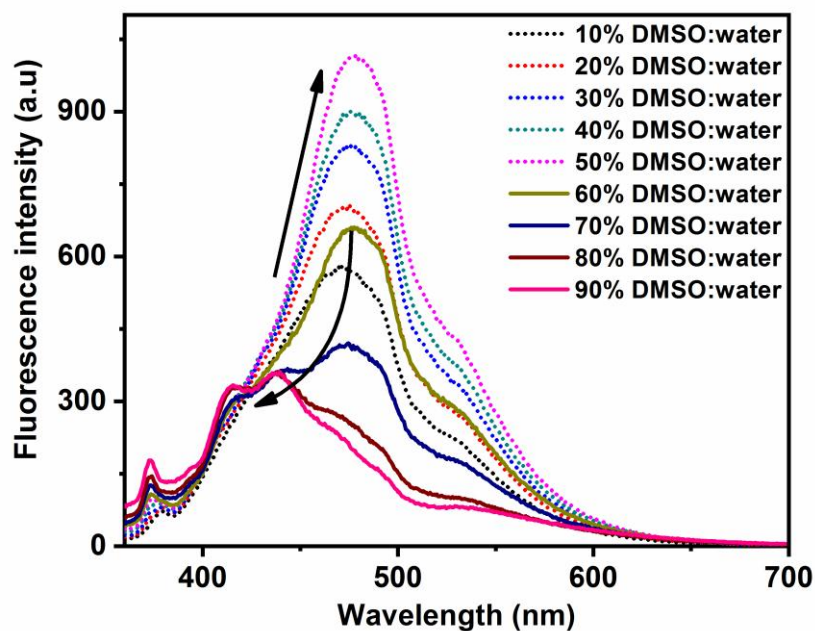


Fig. S16. Fluorescence spectra of L (50 μM) in various ratios (v/v) of DMSO and water in HEPES buffered medium (pH = 8.0).

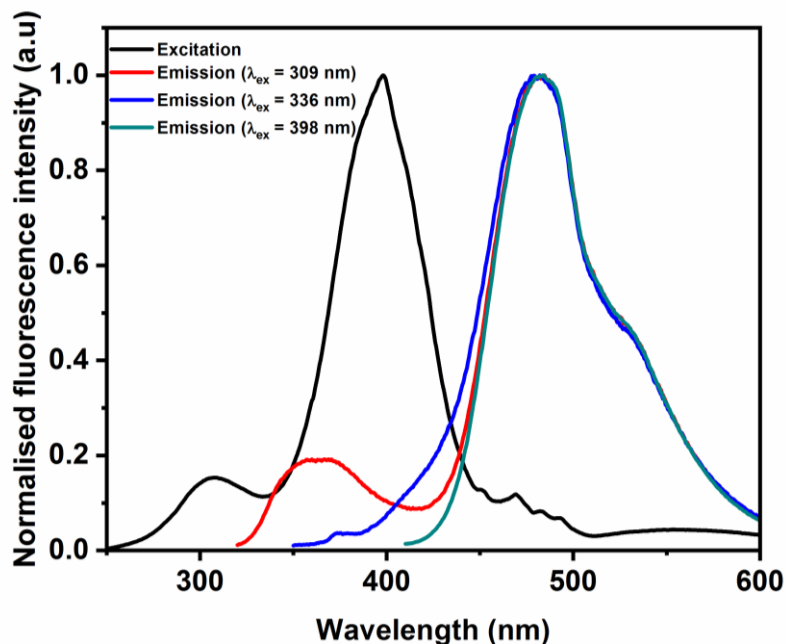


Fig. S17. Normalised excitation and emission spectra of probe, **L** ($\lambda_{\text{ex}} = 309, 336$ and 398 nm).

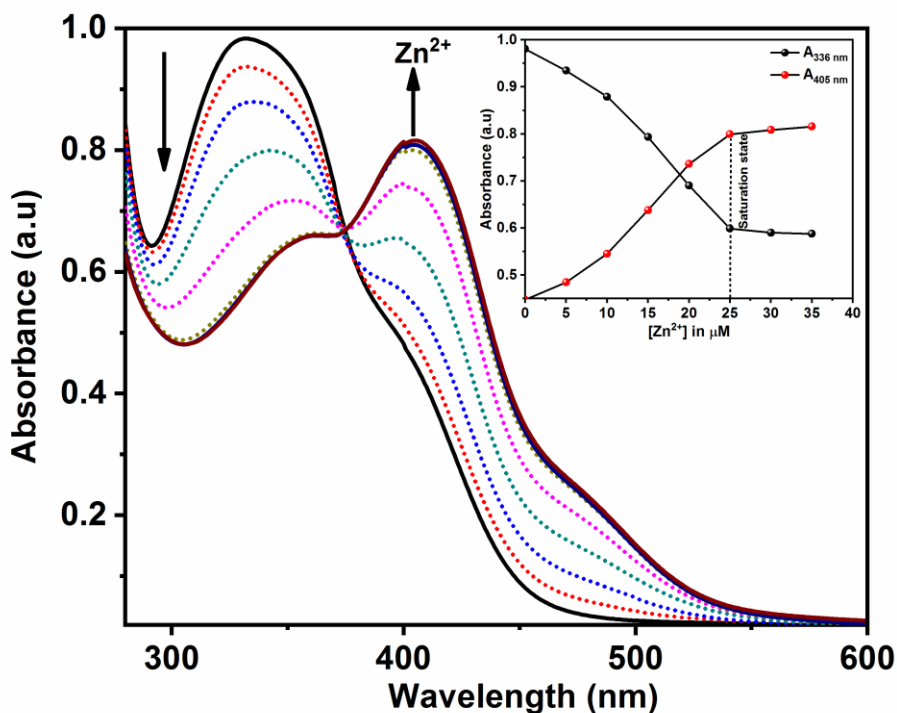


Fig. S18. UV-Vis titration of **L** ($50 \mu\text{M}$) in HEPES buffered ($\text{pH} = 8.0$) (DMSO:water (1:1, v/v)) medium upon addition of Zn^{2+} ; gradually increasing $[\text{Zn}^{2+}]$ from 0 to $25 \mu\text{M}$, excess addition till $35 \mu\text{M}$. Inset: The plot of absorbance intensity at 405 and 336 nm versus concentration of Zn^{2+} .

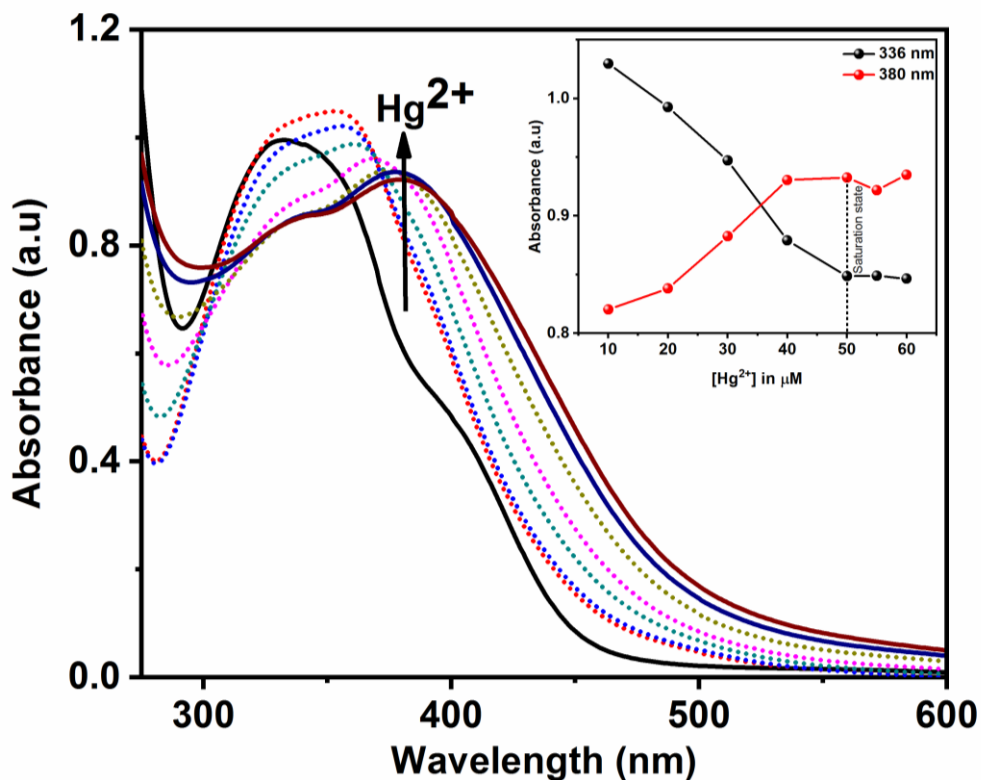


Fig. S19. UV-Vis titration of L (50 μM) in HEPES buffered (pH = 8.0) (DMSO:water (1:1, v/v)) medium upon addition of Hg²⁺; gradually increasing [Hg²⁺] from 0 to 50 μM, and excess addition till 60 μM. Inset: The plot of absorbance intensity at 388 and 336 nm versus concentration of Hg²⁺.

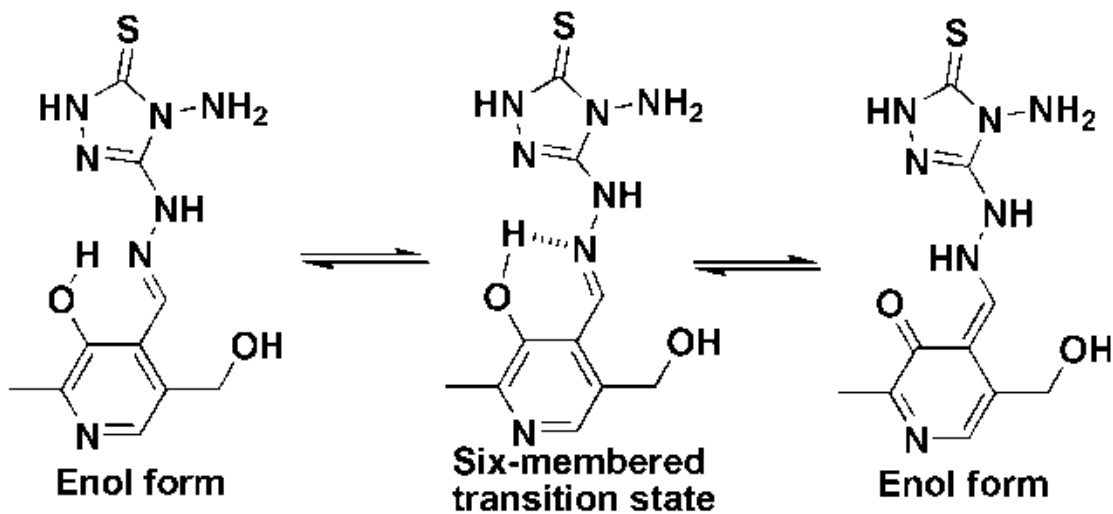


Fig. S20. Illustration of keto-enol tautomerism *via* six-membered transition state.

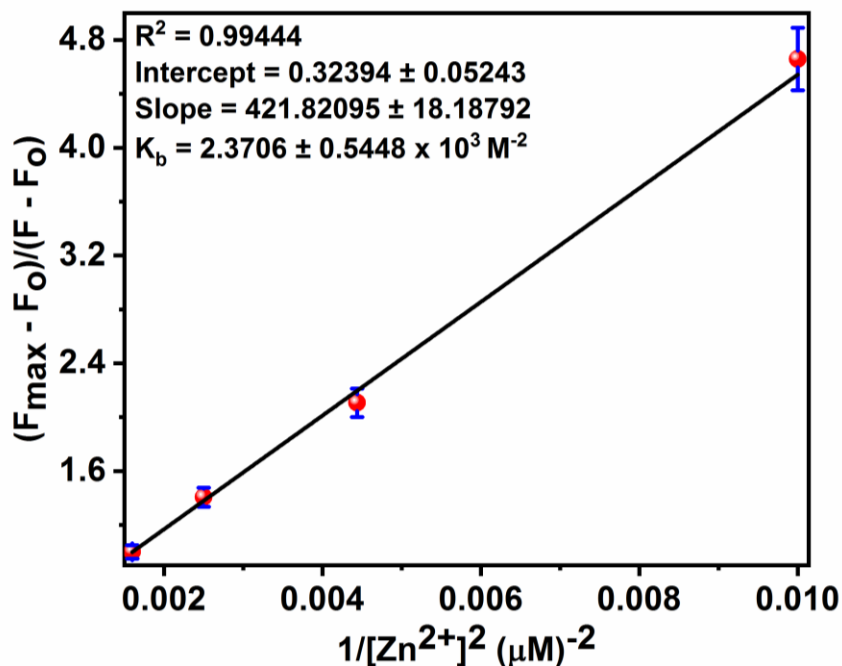


Fig. S21. Benesi-Hildebrand (B-H) plot of fluorescence changes at 440 nm upon addition of Zn^{2+} ion (linearity plotted using the addition from 10 μM to 25 μM of Zn^{2+} to **L**).

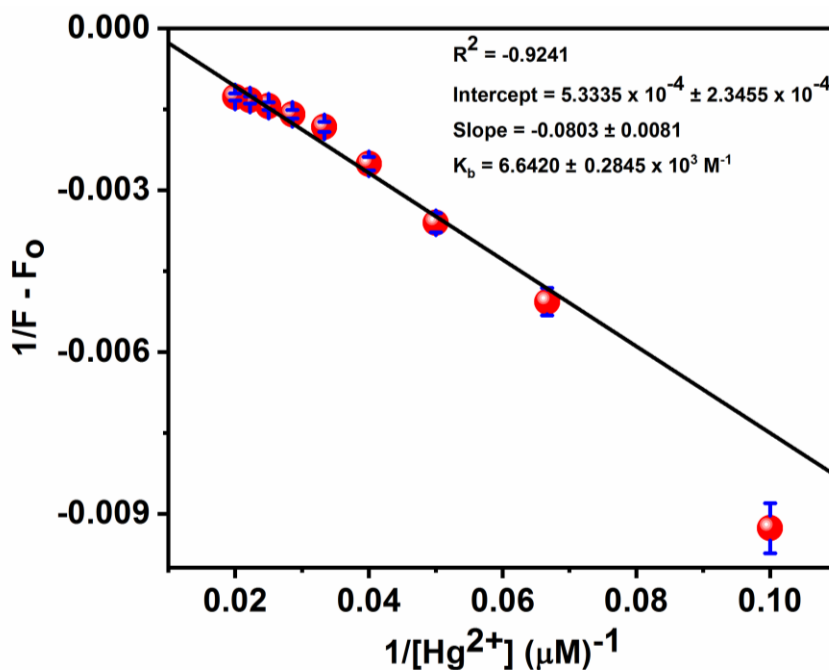


Fig. S22. Benesi-Hildebrand (B-H) plot of fluorescence changes at 478 nm upon addition of Hg^{2+} ion (linearity plotted using the addition from 10 μM to 50 μM of Hg^{2+} to **L**).

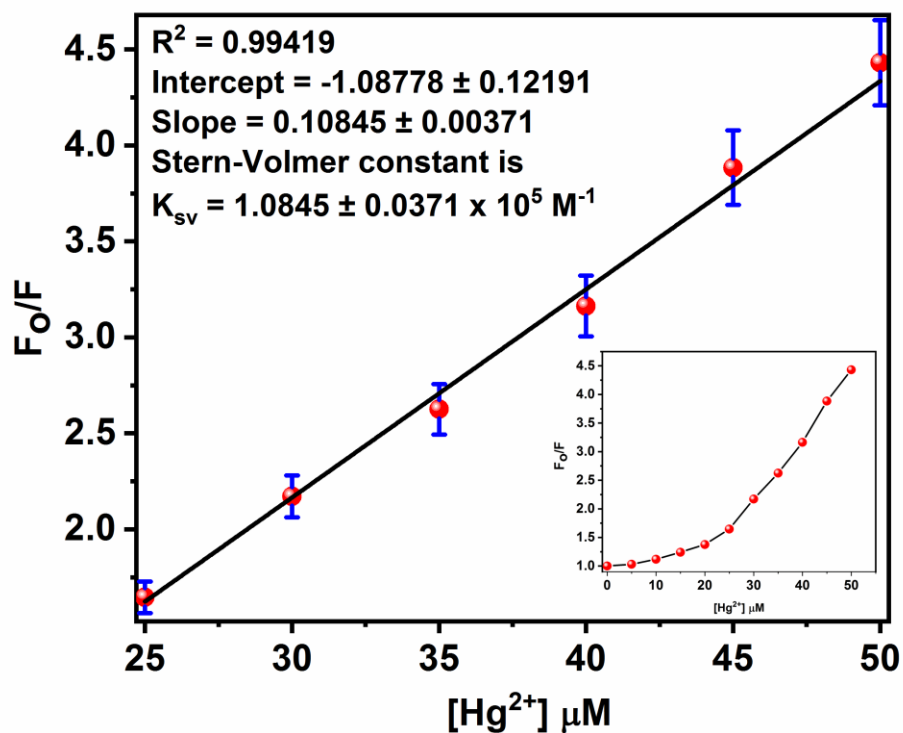


Fig. S23. Stern-Volmer plot of fluorescence changes at 478 nm upon addition of Hg^{2+} ion (linearity plotted using the addition from 25 μM to 50 μM of Hg^{2+} to L).

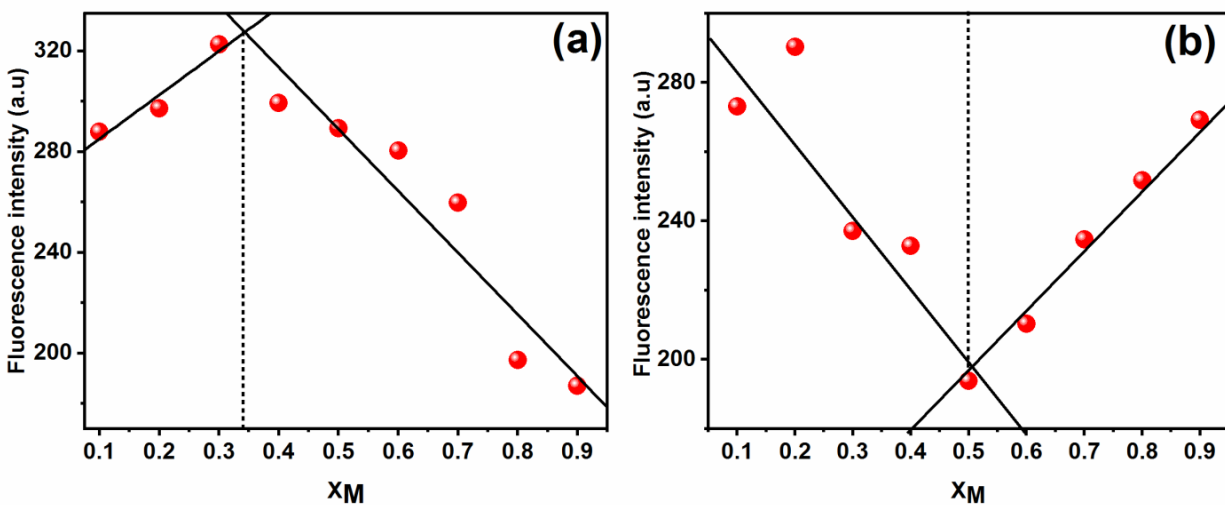


Fig. S24. Job's plot for (a) ZnL_2 and (b) Hg_2L_2 formation using emission spectral data of ($\lambda_{ex} = 336 \text{ nm}$).

Calculation of Limit of Detection (LOD)

The limit of detection (LOD) was estimated based on emission titration data. The detection limit was calculated using equation (7),

$$\text{LOD} = \frac{3\sigma}{k} \quad \dots(7)$$

Where, σ is the standard deviation of blank measurement^[7] and k is the slope between fluorescence intensity versus respective metal ion concentration.

Limit of detection is determined using fluorescence method. Standard deviation is calculated from of free ligand (without zinc) measured its fluorescence intensity with five times and shows standard deviation of 5.7060.

The slope of 32.76126 ± 11.2278 is obtained from linear regressive plot of increasing zinc ion concentration of fixed probe concentration (50 μM). From which, we calculated using standard formula $\text{LOD} = 3 \times 5.7060 / 32.76126 \pm 11.2278 = 5.225 \pm 0.1530 \times 10^{-7}$ M. Similarly, using the slope value obtained from linear regressive plot of increasing mercury ion concentration of fixed probe concentration and calculated LOD is $10.592 \pm 0.734 \times 10^{-7}$ M.

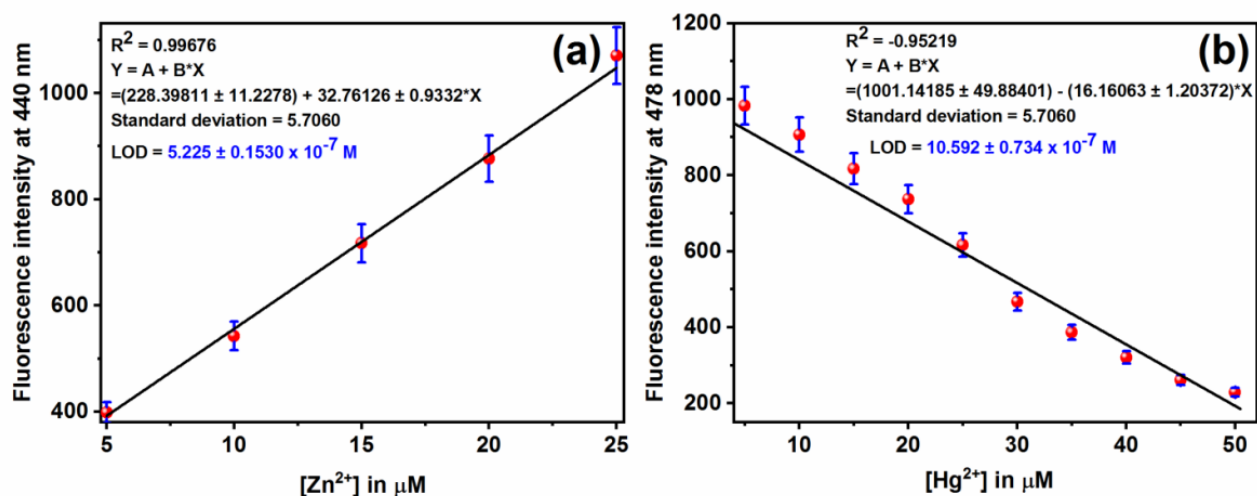


Fig. S25. Determination of LOD (a) Linear regressive plot of **L** with Zn²⁺ ion concentration from 5 to 25 μM (b) Linear regressive plot of **L** with Hg²⁺ ion concentration from 5 to 50 μM .

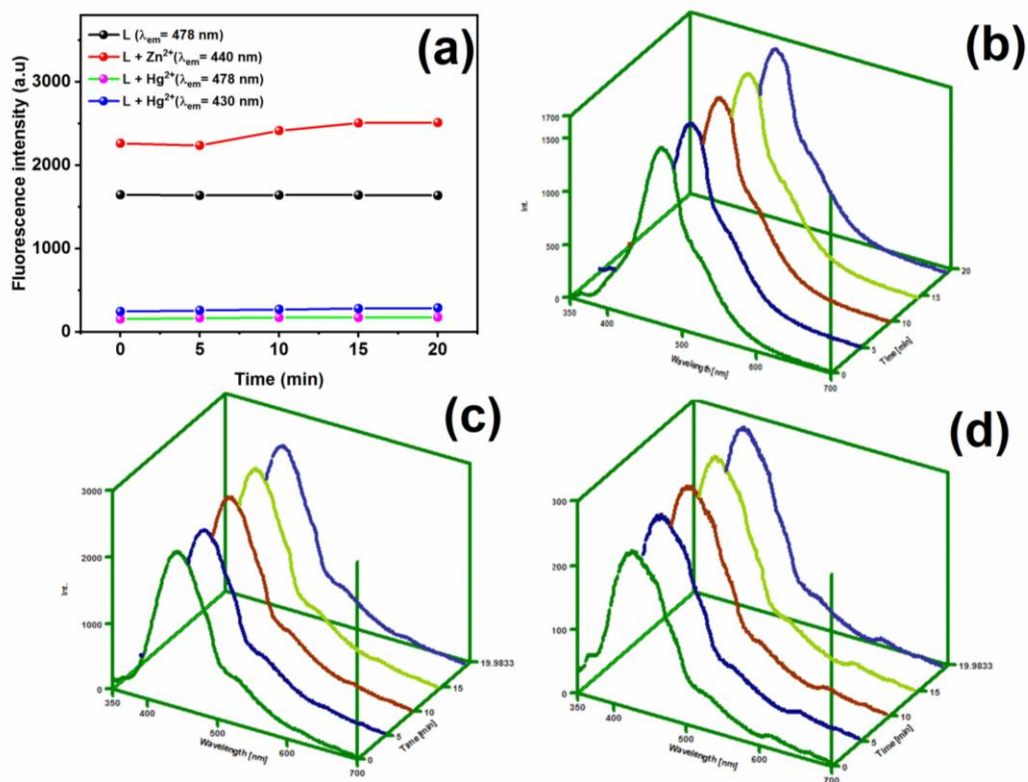


Fig. S26. (a) Time course measurement study of **L** (60 μ M) in the presence and absence of Zn^{2+} and Hg^{2+} (60 μ M); The full spectrum viewed and labeled as (b), (c) and (d) are 3D plot of interval scan measurements of **L**, **L** + Zn^{2+} and **L** + Hg^{2+} in HEPES buffered (pH = 8.0) (DMSO:water (1:1, v/v)) medium.

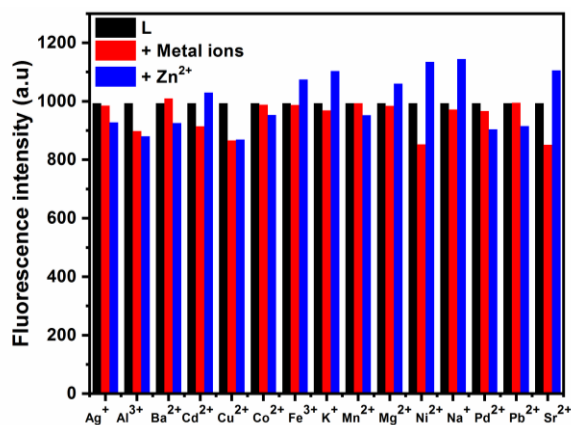


Fig. S27. Fluorescence Interference study of **L** in the presence of competitive metal ions (1 equiv.) with and without Zn^{2+} ion (1.0 equiv.) HEPES buffered (pH = 8.0) (DMSO:water (1:1, v/v)).

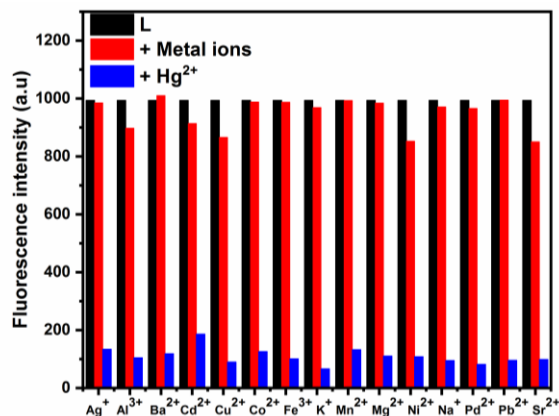


Fig. S28. Fluorescence Interference study of **L** in the presence of competitive metal ions (1 equiv.) with and without Hg^{2+} ion (1 equiv.) HEPES buffered (pH = 8.0) (DMSO:water (1:1, v/v)).

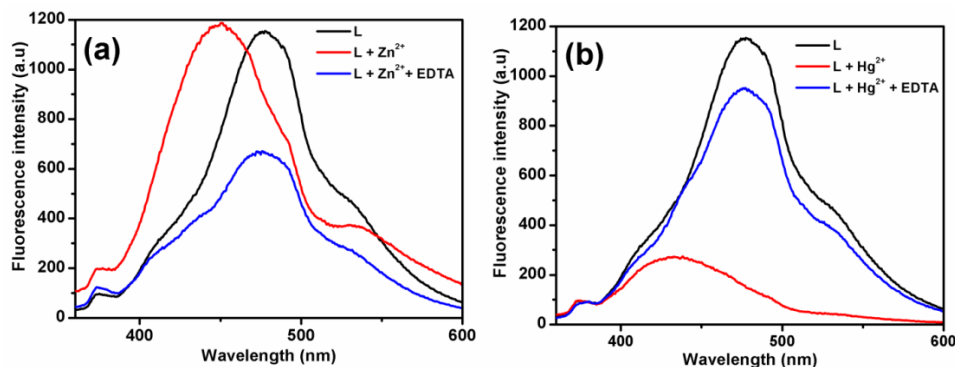


Fig. S29. Fluorescence spectra recorded in HEPES buffered (pH = 8.0) DMSO:water (1:1, v/v) medium; (a) Reversibility of **L** + Zn^{2+} with EDTA (b) Reversibility of **L** + Hg^{2+} with EDTA.

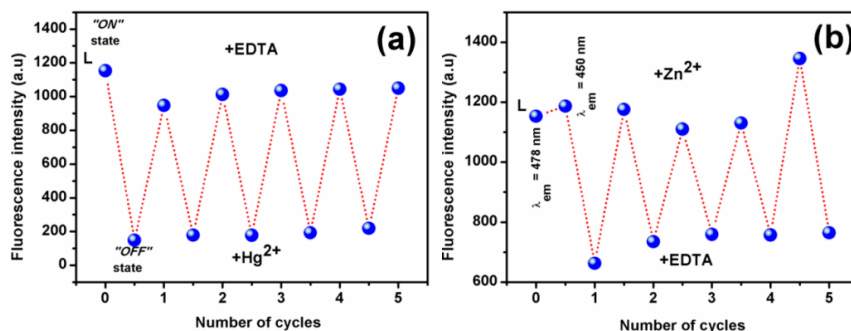


Fig. S30. Recovery cycles of (a) **L** (50 μM) upon alternative addition of Zn^{2+} (1 equiv.) and EDTA (1 equiv.); (b) **L** (50 μM) upon alternative addition of Zn^{2+} (1 equiv.) and EDTA (1 equiv.)

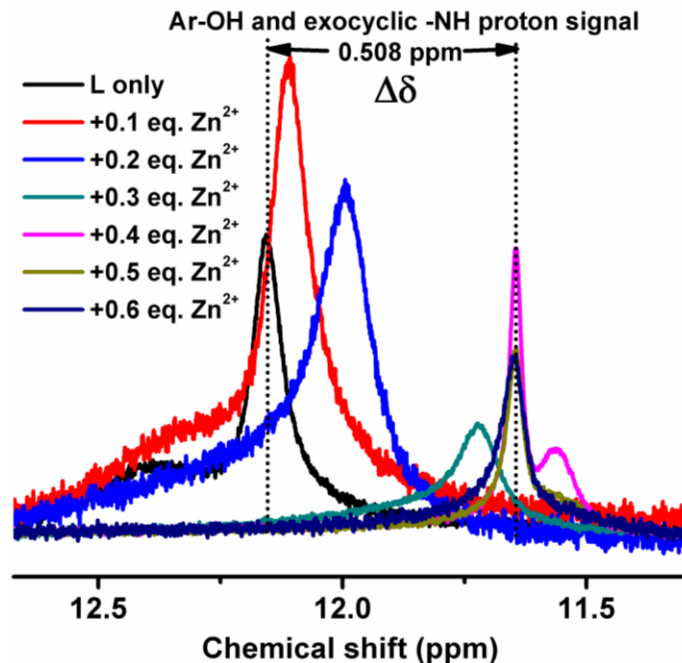


Fig. S31. Partial ¹H NMR spectral titration of probe with successive addition of Zn(OAc)₂ in DMSO-*d*₆ for zoomed view of aromatic -OH and exocyclic -NH signal changes.

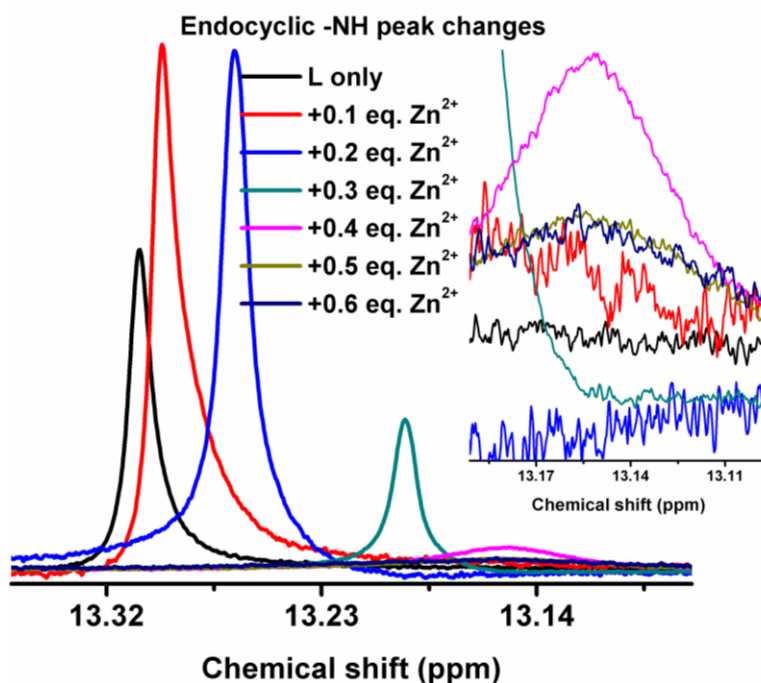


Fig. S32. Partial ¹H NMR spectral titration of probe with successive addition of Zn(OAc)₂ in DMSO-*d*₆ for zoomed view of endocyclic -NH signal changes.

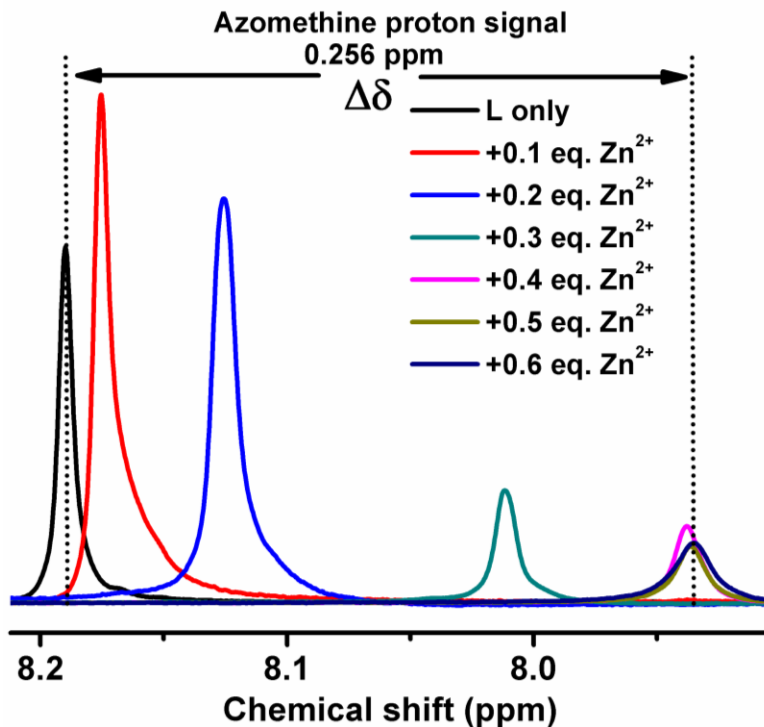


Fig. S33. Partial ¹H NMR spectral titration of probe with successive addition of Zn(OAc)₂ in DMSO-*d*₆ for zoomed view of azomethine signal changes.

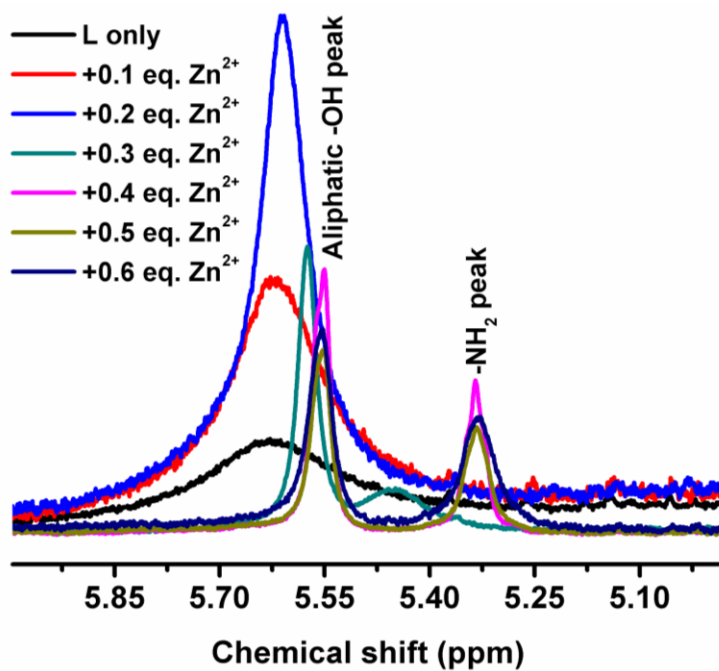


Fig. S34. Partial ¹H NMR spectral titration of probe with successive addition of Zn(OAc)₂ in DMSO-*d*₆ for zoomed view of aliphatic -OH and -NH₂ signal changes.

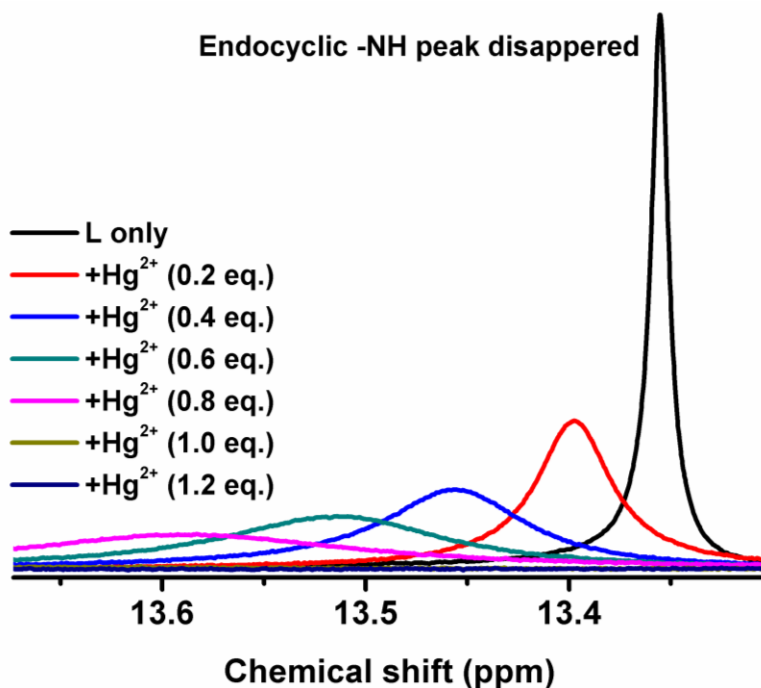


Fig. S35. Partial ¹H NMR spectral titration of probe with successive addition of HgCl₂ in DMSO-*d*₆ for zoomed view of endocyclic -NH signal changes.

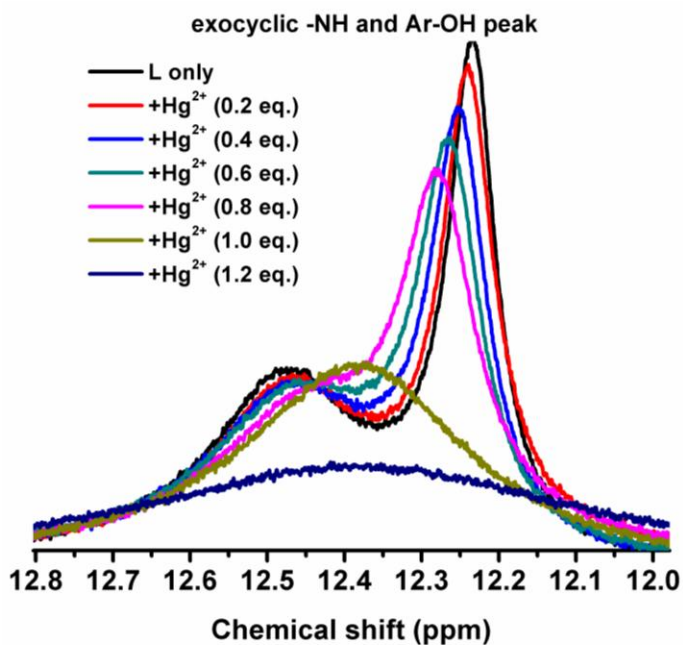


Fig. S36. Partial ¹H NMR spectral titration of probe with successive addition of HgCl₂ in DMSO-*d*₆ for zoomed view of exocyclic -NH and Ar-OH signal changes.

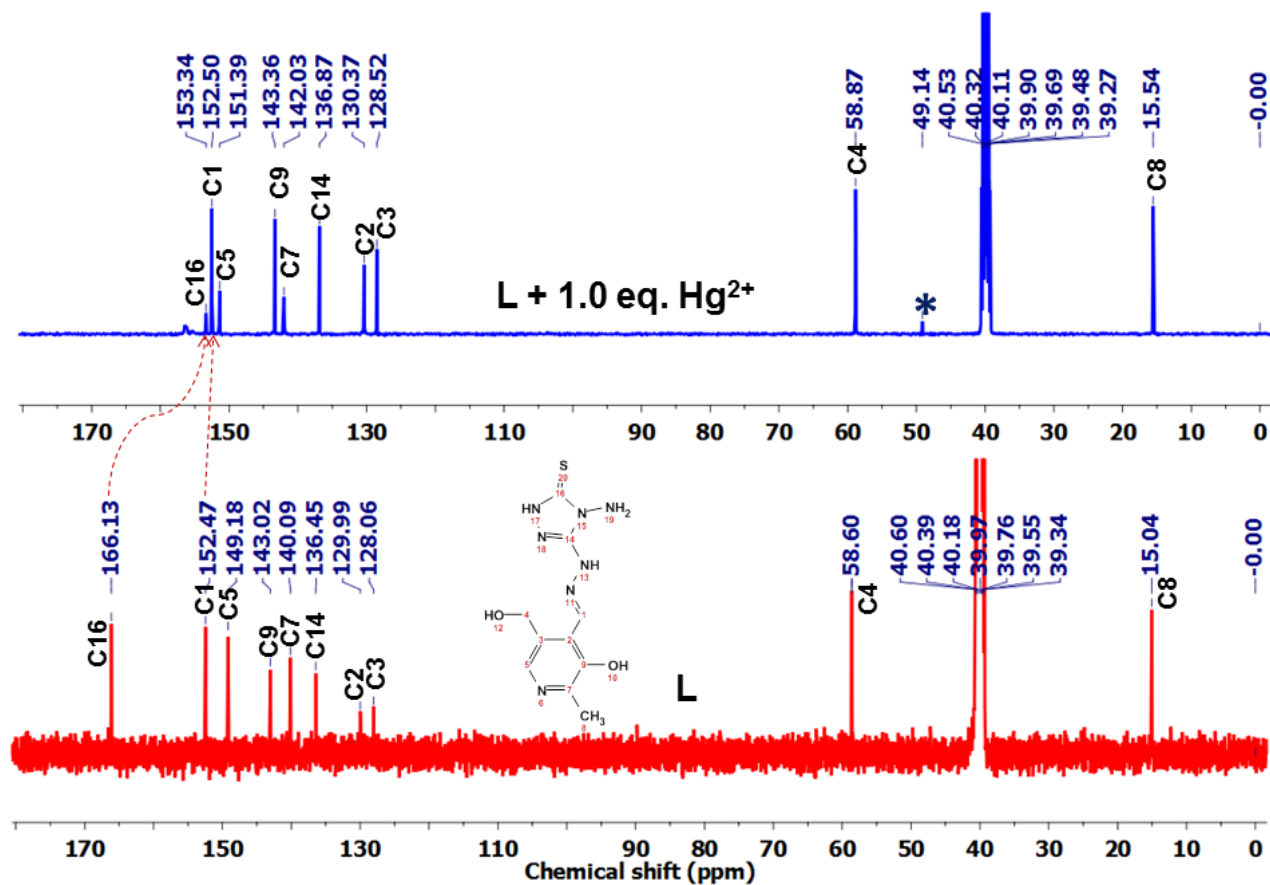


Fig. S37. ¹³C NMR spectra of probe (L) with 1.0 equivalent addition of HgCl₂ in DMSO-*d*₆ (100 MHz) Note; the asterisk symbol * indicated that trace amount of methanol solvent.

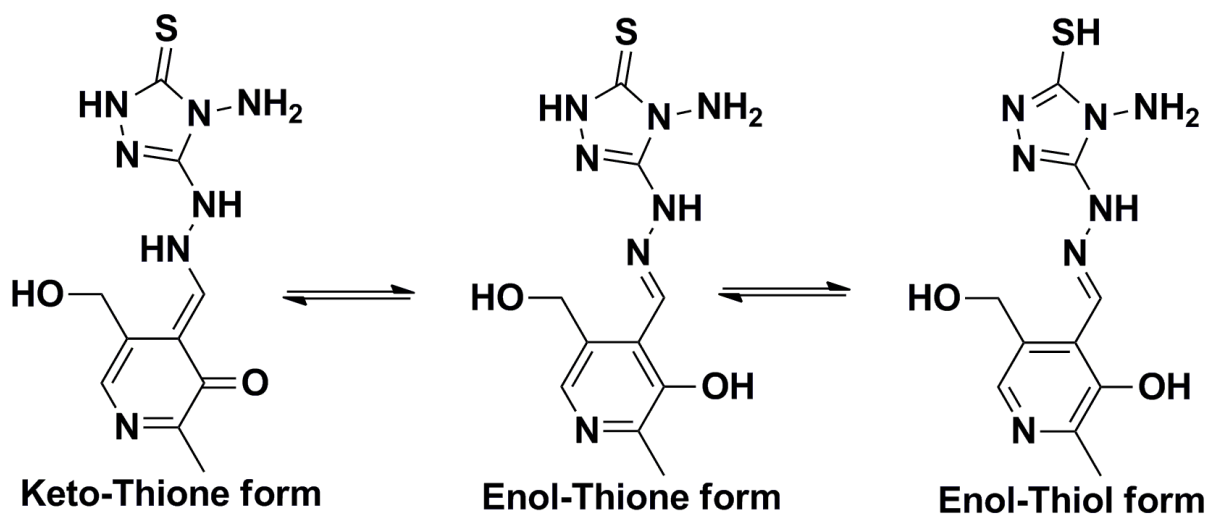


Fig. S38. Possible tautomeric forms of probe (L).

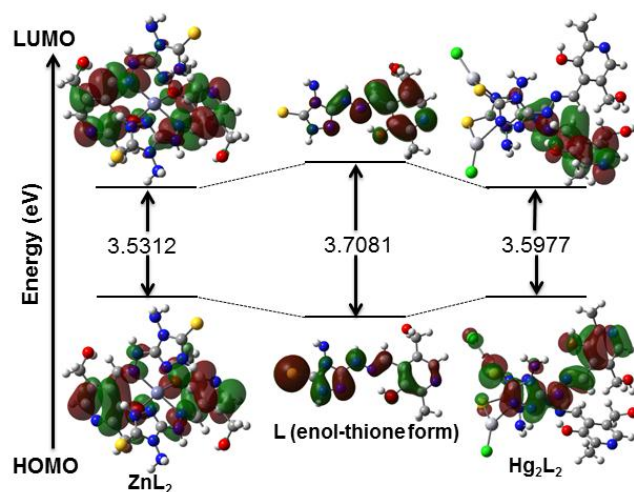


Fig. S39. Frontier molecular orbital diagram of **L**, **ZnL₂** and **Hg₂L₂** in gas phase level.

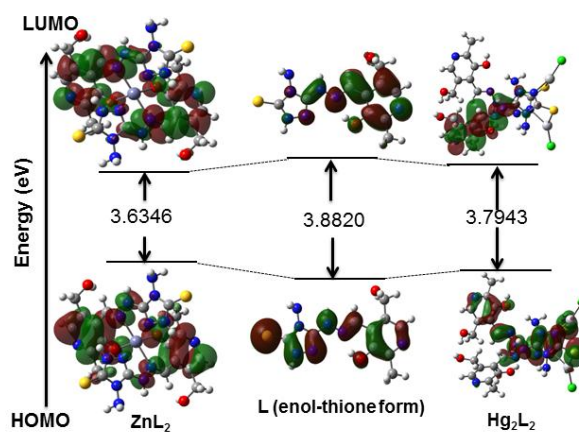


Fig. S40. Frontier molecular orbital diagram of **L**, **ZnL₂** and **Hg₂L₂** in water medium.

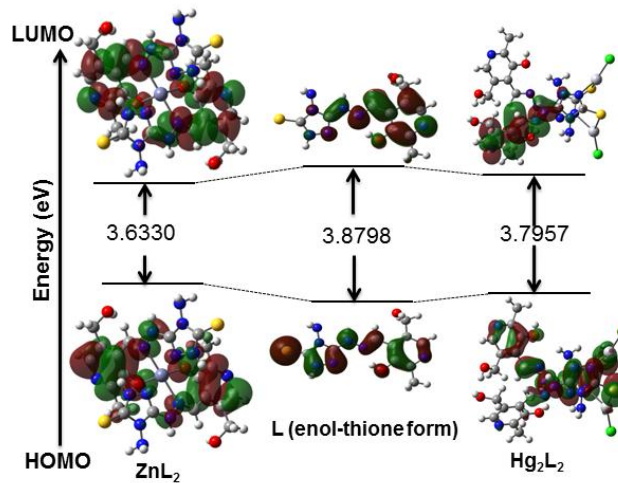


Fig. S41. Frontier molecular orbital diagram of **L**, **ZnL₂** and **Hg₂L₂** in DMSO medium.

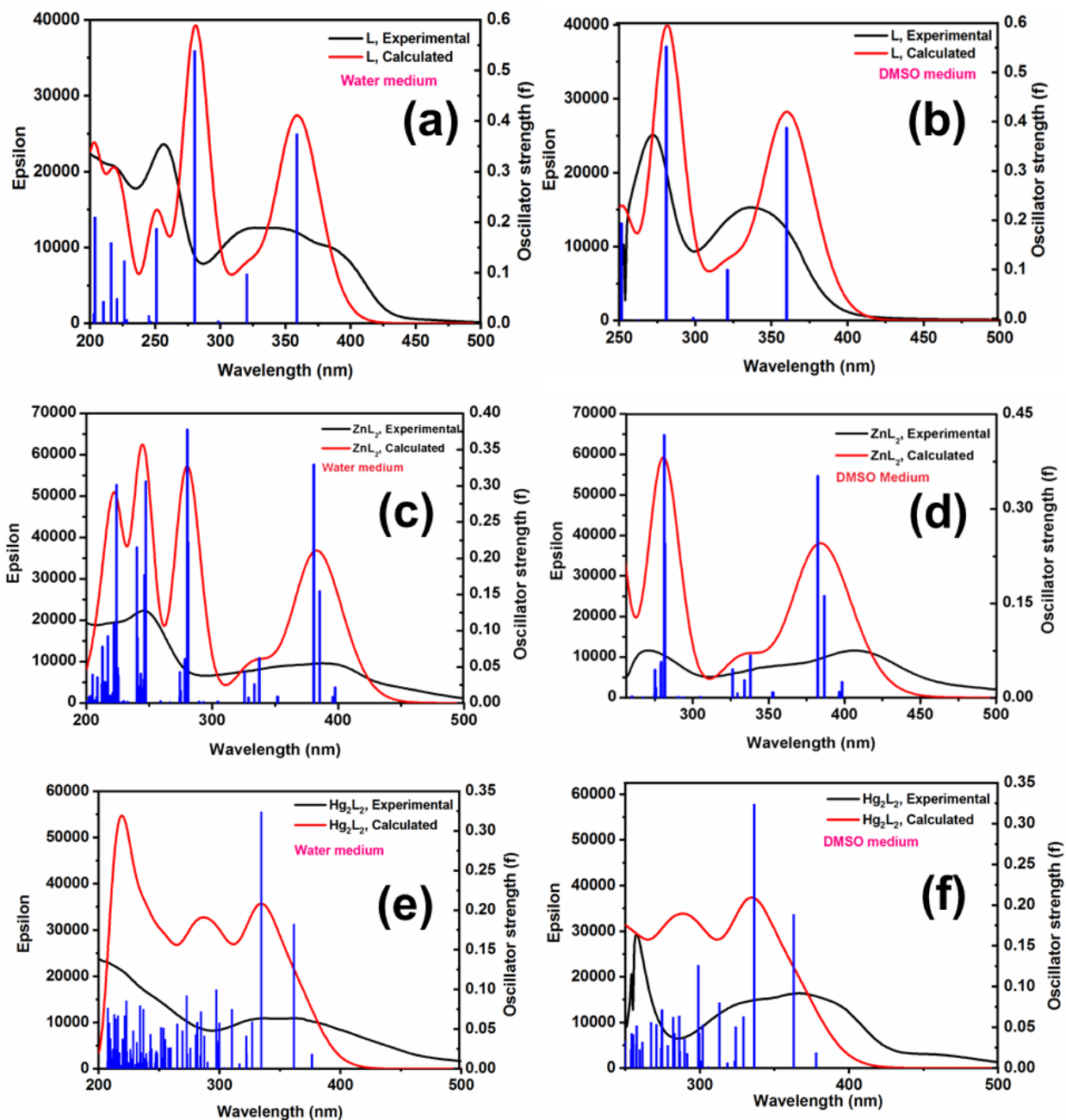


Fig. S42. Calculated UV-Vis spectra (red colour) with oscillator strengths (blue colour) of (a) **L** in water (b) **L** in DMSO (c) **ZnL₂** in water (d) **ZnL₂** in DMSO (e) **Hg₂L₂** in water and (f) **Hg₂L₂** in DMSO medium; The black colour represents the experimental UV-Vis results.

To determine the optical band gap of probe, and its complexes with Zn²⁺ and Hg²⁺, the solid state UV-DRS spectra were analysed. The optical band gap was calculated from Tauc plot by

extrapolating the linear to x-axis, i.e., $[hvF(R)]^{1/2} = 0$ (Fig. S43). It has been noted that the optical band gap of probe (2.406 eV) was reduced to 2.0392 and 1.9595 eV, respectively, for the mixtures of **L** + **Zn(II)** and **L** + **Hg(II)**. The complex formation was confirmed by the decreased optical band gaps of probe with Zn^{2+} and Hg^{2+} . This experimentally observed band gaps for probe and its complexes were found to be lesser than the theoretical values. They were calculated using HOMO-LUMO energy gap of optimized geometries in gas phase (Fig. S39). The deviation in band gap may be due to the comparison of solid-state measurement with the gas phase optimized geometries.^[8]

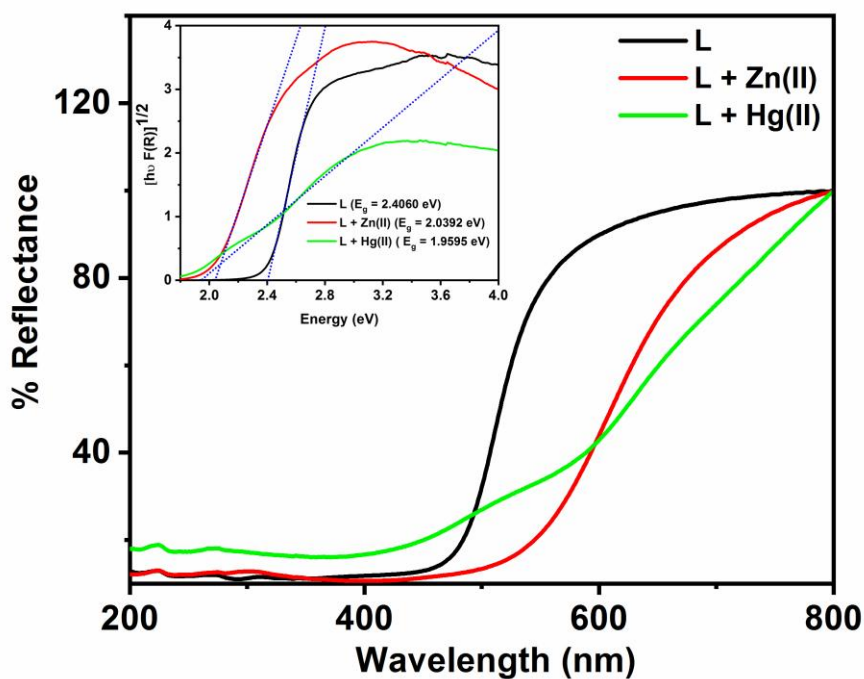


Fig. S43. Solid state UV-DRS spectra of **L**, **L** + **Zn(II)** and **L** + **Hg(II)**, Inset: Kubelka–Munk (K–M) plot used for band gap calculations.

The Hirshfeld surface analysis

Hirshfeld surface analysis generates pictorial representations of intercontacts, molecular shapes, and intermolecular interactions within crystal packings. Hirshfeld surfaces and 2D fingerprint plots are used to gain a better understanding of short-range intermolecular forces in

crystal structures, as well as information about the relative surface area corresponding to each type of interaction.^[9] The Hirshfeld surface areas were distributed over d_i (0.750 to 2.500 Å), d_e (0.750 to 2.500 Å), d_{norm} (-0.650 to 1.100 Å), shape index (-1.000 to 1.000 Å) and curvedness (-4.900 to 0.390 Å) (Fig. S44). The surface plot displayed by d_{norm} indicated the strongest (red colour), intermediate (white), and weakest intermolecular (blue) interactions. The hydrogen bonding interactions were indicated as red spots (d_{norm}) as shown in Fig. 44c. The existence of red and blue triangles (highlighted) in the shape index (Fig. 44d) shows the presence of π - π interactions. A lower number of blue and red triangles clearly indicated the weak π - π interactions.^[10] The intermolecular interactions of probe (**L**) are given in the 2D fingerprint plots (Fig. S45). The major H-H (41.9 %) contacts make the largest contribution to the Hirshfeld surfaces. The heteroatomic interactions of C-H (7.1 %), N-H (10.7 %), O-H (17.6 %) and S-H (12.5 %) which include all reciprocal contacts contributes to the Hirshfeld surface.

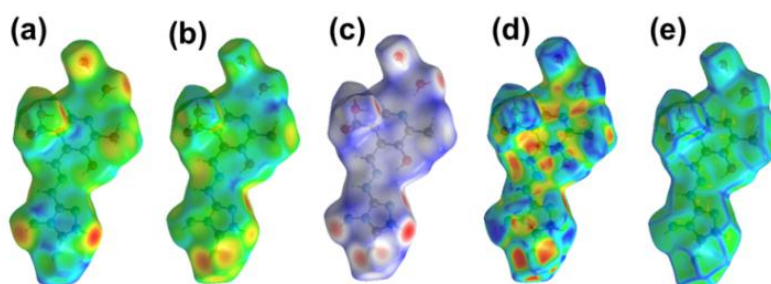


Fig. S44. Hirshfeld surfaces mapped over (a) d_i ; (b) d_e ; (c) d_{norm} ; (d) shape index; and (e) curvedness for probe (**L**).

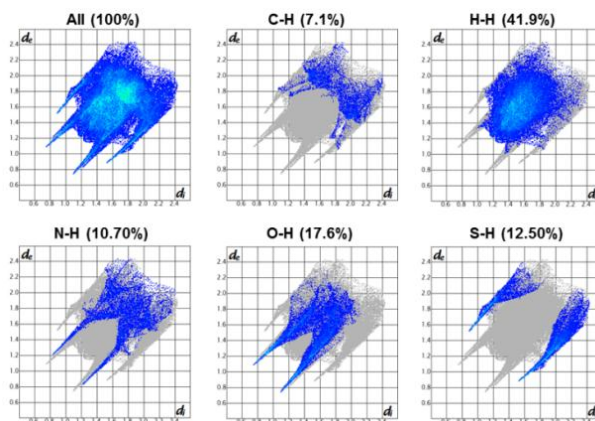


Fig. S45. Two-dimensional fingerprint (2D) plots of probe (**L**) generated from Crystal Explore software.

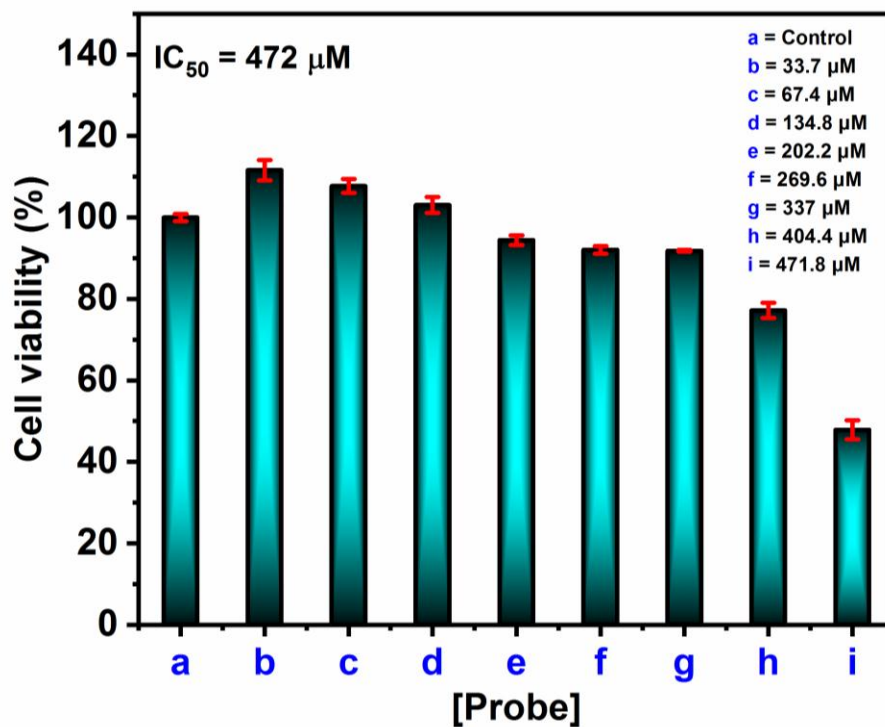


Fig. S46. Determination of cytotoxicity of L on A549 cells by MTT assay.

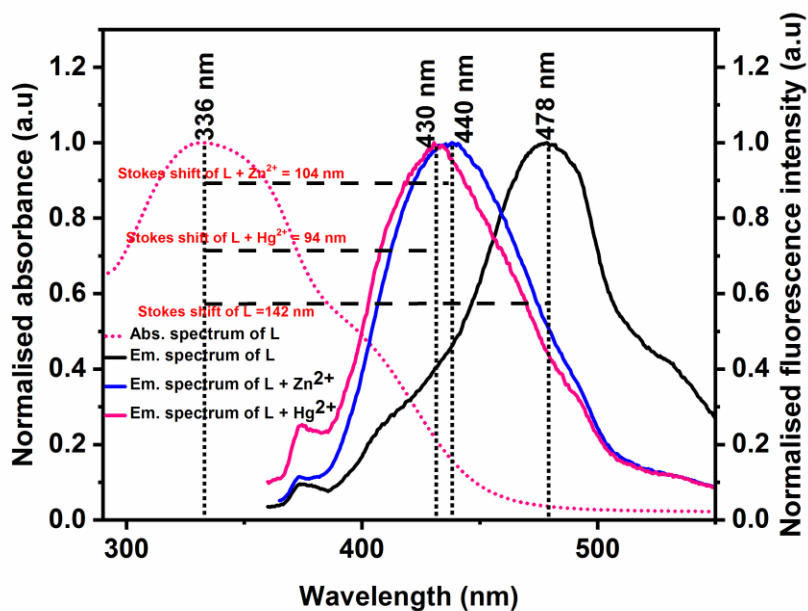


Fig. S47. Comparison plot of normalized absorbance and emission spectra of L, L + Zn²⁺ and L + Hg²⁺ (Stokes shift analysis).

Table S1. FT-IR assignments of **L**, **L + Zn²⁺** and **L + Hg²⁺**.

S. No.	Vibrational frequency, ν (cm ⁻¹)			Vibrational assignment
	L	L + Zn²⁺	L + Hg²⁺	
1.	3446	overtone	3455	$\nu(\text{OH})$
2.	3324		overtone	$\nu_{\text{as}}(\text{N-H})_{\text{amino}}$
3.	3206			$\nu_{\text{s}}(\text{N-H})_{\text{amino}}$
4.	3093			$\nu(\text{N-H})_{\text{hydrazino}}$
5.	1626	1650	1694	$\nu(\text{C=N})_{\text{azomethine}}$
6.	1477	1596	1538	$\nu(\text{C=N})_{\text{triazole}}$
7.	1425	1417	1448	Thioamide I, $\delta(\text{N-H}) + \nu(\text{C-N})$
8.	1291	1220	1193	Thioamide II, $\nu(\text{C=S}) + \nu(\text{C-N}) + \delta(\text{N-H})$
9.	1016	1018	1009	Thioamide III, $\nu(\text{C-N})_{\text{major}} + \nu(\text{C=S})_{\text{minor}}$
10.	883	865	846	Thioamide IV, $\nu(\text{C=S})$
N-H and O-H vibrational bands in complex were observed overtone with each others				

Table S2. Crystal data and structure refinement for **L**.

Empirical formula	C ₁₀ H ₁₉ N ₇ O ₅ S	
Formula weight	349.38	
Temperature	296(2) K	
Wavelength	0.71073 Å	
Crystal system	Triclinic	
Space group	P -1	
Unit cell dimensions	a = 6.8490(2) Å	$\alpha = 92.744(2)^\circ$.
	b = 9.0017(2) Å	$\beta = 98.751(2)^\circ$.
	c = 14.0341(3) Å	$\gamma = 112.305(2)^\circ$.
Volume	785.88(4) Å ³	
Z	2	
Density (calculated)	1.476 Mg/m ³	
Absorption coefficient	0.244 mm ⁻¹	
F(000)	368	
Crystal size	0.120 x 0.100 x 0.080 mm ³	
Theta range for data collection	2.462 to 24.992°.	
Index ranges	-8 ≤ h ≤ 8, -10 ≤ k ≤ 10, -16 ≤ l ≤ 16	
Reflections collected	9992	
Independent reflections	2774 [R(int) = 0.0248]	

Completeness to theta = 24.992°	100.0 %
Absorption correction	Semi-empirical from equivalents
Max. and min. transmission	1.00000 and 0.77803
Refinement method	Full-matrix least-squares on F ²
Data / restraints / parameters	2774 / 1 / 247
Goodness-of-fit on F ²	1.077
Final R indices [I>2sigma(I)]	R1 = 0.0357, wR2 = 0.0940
R indices (all data)	R1 = 0.0403, wR2 = 0.0980
Extinction coefficient	n/a
Largest diff. peak and hole	0.235 and -0.279 e.Å ⁻³

Table S3. Bond lengths [Å] and angles [°] for **L**.

C(1)-N(1)	1.341(2)
C(1)-C(2)	1.373(2)
C(1)-H(1A)	0.93
C(2)-C(3)	1.405(2)
C(2)-C(7)	1.511(2)
C(3)-C(4)	1.403(2)
C(3)-C(8)	1.451(2)
C(4)-O(2)	1.351(2)
C(4)-C(5)	1.397(2)
C(5)-N(1)	1.332(2)
C(5)-C(6)	1.497(2)
C(6)-H(6A)	0.96
C(6)-H(6B)	0.96
C(6)-H(6C)	0.96
C(7)-O(1)	1.424(2)
C(7)-H(7A)	0.97
C(7)-H(7B)	0.97
C(8)-N(2)	1.279(2)
C(8)-H(8)	0.93
C(9)-N(4)	1.301(2)
C(9)-N(3)	1.349(2)
C(9)-N(6)	1.364(2)
C(10)-N(5)	1.316(2)
C(10)-N(6)	1.372(2)
C(10)-S(1)	1.6789(18)

N(2)-N(3)	1.3595(19)
N(3)-H(3)	0.86
N(4)-N(5)	1.387(2)
N(5)-H(5)	0.91(2)
N(6)-N(7)	1.3959(19)
N(7)-H(8B)	0.8615
N(7)-H(8A)	0.89(2)
O(1)-H(1)	0.74(2)
O(2)-H(2)	0.82
O(3)-H(3A)	0.81(3)
O(3)-H(3B)	0.81(4)
O(4)-H(4A)	0.84(3)
O(4)-H(4B)	0.853(19)
O(5)-H(5A)	0.81(3)
O(5)-H(5B)	0.84(3)
N(1)-C(1)-C(2)	124.22(17)
N(1)-C(1)-H(1A)	117.9
C(2)-C(1)-H(1A)	117.9
C(1)-C(2)-C(3)	118.45(15)
C(1)-C(2)-C(7)	119.81(16)
C(3)-C(2)-C(7)	121.72(15)
C(4)-C(3)-C(2)	117.18(15)
C(4)-C(3)-C(8)	121.63(15)
C(2)-C(3)-C(8)	121.18(15)
O(2)-C(4)-C(5)	116.43(15)
O(2)-C(4)-C(3)	123.33(15)
C(5)-C(4)-C(3)	120.23(16)
N(1)-C(5)-C(4)	121.44(15)
N(1)-C(5)-C(6)	118.78(16)
C(4)-C(5)-C(6)	119.77(17)
C(5)-C(6)-H(6A)	109.5
C(5)-C(6)-H(6B)	109.5
H(6A)-C(6)-H(6B)	109.5
C(5)-C(6)-H(6C)	109.5
H(6A)-C(6)-H(6C)	109.5
H(6B)-C(6)-H(6C)	109.5
O(1)-C(7)-C(2)	113.32(15)
O(1)-C(7)-H(7A)	108.9
C(2)-C(7)-H(7A)	108.9
O(1)-C(7)-H(7B)	108.9
C(2)-C(7)-H(7B)	108.9

H(7A)-C(7)-H(7B)	107.7
N(2)-C(8)-C(3)	119.25(15)
N(2)-C(8)-H(8)	120.4
C(3)-C(8)-H(8)	120.4
N(4)-C(9)-N(3)	126.74(15)
N(4)-C(9)-N(6)	111.62(15)
N(3)-C(9)-N(6)	121.64(14)
N(5)-C(10)-N(6)	103.44(15)
N(5)-C(10)-S(1)	128.44(14)
N(6)-C(10)-S(1)	128.12(13)
C(5)-N(1)-C(1)	118.46(15)
C(8)-N(2)-N(3)	119.03(14)
C(9)-N(3)-N(2)	115.88(13)
C(9)-N(3)-H(3)	122.1
N(2)-N(3)-H(3)	122.1
C(9)-N(4)-N(5)	102.70(14)
C(10)-N(5)-N(4)	114.21(15)
C(10)-N(5)-H(5)	127.6(15)
N(4)-N(5)-H(5)	117.4(15)
C(9)-N(6)-C(10)	108.03(13)
C(9)-N(6)-N(7)	122.74(14)
C(10)-N(6)-N(7)	129.12(14)
N(6)-N(7)-H(8B)	109.3
N(6)-N(7)-H(8A)	105.6(15)
H(8B)-N(7)-H(8A)	112.6
C(7)-O(1)-H(1)	110.4(18)
C(4)-O(2)-H(2)	109.5
H(3A)-O(3)-H(3B)	106(3)
H(4A)-O(4)-H(4B)	102(3)
H(5A)-O(5)-H(5B)	107(3)

Symmetry transformations used to generate equivalent atoms

Table S4. Summarized λ_{max} (nm) emission data of **L** in various solvents.

	ACN	DMF	DMSO	MeOH	Water	Buffer
L	550 nm	429 nm	426 nm	425 nm	379 nm	480 nm

Table S5. Summarized λ_{max} (nm) emission data of **L** in various ratios (v/v) of DMSO and water in HEPES buffered medium (pH = 8.0).

DMSO:water (v/v)	10%	20%	30%	40%	50%	60%	70%	80%	90%
L	470 nm	478 nm	478 nm	478 nm	478 nm	477 nm	474 nm	438 nm	439 nm
Intensity (a.u)	573.404	706.404	829.842	896.842	1015.97	660.167	420.247	361.303	360.999

Table S6. Solid and solution state fluorescence lifetime data of **L**, **ZnL₂**, and **Hg₂L₂**.

	B₁	B₂	B₃	τ_1 (ns)	τ_2 (ns)	τ_3 (ns)	χ^2	τ_{av} (ns)	Φ_f	k_r (ns⁻¹)	k_{nr} (ns⁻¹)	$\frac{k_r}{k_{\text{nr}}}$
(a) Solution state lifetime data												
L	0.1175	0.0105	0.1129	2.6466	4.0472	0.1821	1.2529	1.5536	0.2316	0.1490	0.4946	0.3012
L + Zn(II)	0.3388	0.5013	0.0094	1.1272	3.0904	13.2159	1.1577	2.4201	0.3850	0.1590	0.2542	0.6254
L + Hg(II)	0.0593	0.0077	1.2706×10^7	1.0810	9.0093	0.0066	1.4592	0.0066	0.0416	6.3030	145.2121	0.0434
(b) Solid state lifetime data												
L	0.0135	0.0011	1.9733	6.6721	43.7577	0.4710	1.5795	0.5380			-	
L + Zn(II)	-0.0065	0.0007	0.8111	0.7167	36.9418	0.2063	1.4965	0.2424			-	
L + Hg(II)	0.0290	0.0004	1.1296	0.4856	30.7468	0.1421	1.4697	0.1625			-	

Φ_f = Fluorescence quantum yield determined based on relative standard method (quinine sulfate as standard)

Table S7. The Cartesian coordinates of **L** (enol-thione), **ZnL₂** and **Hg₂L₂** calculated from Gaussian-09 at B3LYP computational level using IEF-PCM calculation (**water as solvent**).

L (enol-thione)				ZnL₂			Hg₂L₂				
C	4.80547	0.48956	-0.15016	C	-4.67713	1.29266	-2.96325	Hg	-3.48257	2.29401	-0.61677
H	5.70724	1.09272	-0.21596	H	-5.53807	1.69471	-3.48958	S	-3.00967	1.48107	1.84359
C	3.56264	1.10067	-0.19737	C	-4.00777	2.06212	-2.03929	N	-0.18996	-1.16572	1.21983
C	2.41274	0.27559	-0.10527	C	-2.87912	1.49236	-1.36954	N	-1.50928	-0.76825	1.21819
C	2.61358	-1.1157	0.00292	C	-2.51691	0.14138	-1.66958	N	-0.3285	0.88352	2.01339
C	3.93311	-1.62828	0.04193	C	-3.3158	-0.53932	-2.66946	N	1.85155	-0.13992	1.95402
C	4.15178	-3.10917	0.17121	C	-2.95284	-1.95227	-3.02718	C	0.49204	-0.16477	1.73181
H	3.69898	-3.64707	-0.66702	H	-3.032	-2.60861	-2.15469	C	-1.59604	0.47863	1.66075
H	3.68253	-3.49823	1.07958	H	-1.91452	-2.01417	-3.3662	Hg	-3.23753	-2.38503	0.50966
H	5.22166	-3.31019	0.1976	H	-3.62049	-2.30723	-3.81131	N	-1.89617	0.91474	-1.93402
C	3.47638	2.59888	-0.37483	C	-4.51309	3.45719	-1.75166	S	-3.89505	-0.85423	-1.49513
H	4.49043	3.00587	-0.46151	H	-5.41667	3.6358	-2.345	Cl	-3.61941	-4.43447	1.81421
H	2.94794	2.85268	-1.29791	H	-4.79141	3.56768	-0.69969	C	-2.25552	-0.34165	-1.75448
C	1.07643	0.85669	-0.10899	C	-2.14615	2.30536	-0.43887	N	-0.53165	0.97868	-2.15014
H	0.99286	1.94358	-0.07816	H	-2.45269	3.34884	-0.3671	C	-0.09357	-0.24518	-2.10556
C	-2.31759	-0.07099	-0.0471	C	0.56969	2.47373	1.73025	N	-1.12747	-1.13252	-1.86223
C	-4.53472	-0.45105	0.00925	C	2.47358	2.56266	2.9263	Cl	-4.67995	4.1365	-1.74909
N	4.99348	-0.83306	-0.03051	N	-4.33844	0.02034	-3.27709	C	6.38558	3.3202	0.1174
N	0.03124	0.10363	-0.09873	N	-1.13325	1.91467	0.27221	C	5.70688	2.15018	0.44199
N	-1.18667	0.69062	-0.08416	N	-0.55655	2.87978	1.0958	C	4.49477	2.25159	1.15792
H	-1.30459	1.69997	-0.07711	H	-0.621	3.86424	0.85406	C	4.05185	3.54281	1.49424
N	-2.41502	-1.3674	-0.0289	N	0.96506	1.23167	1.81671	C	4.82186	4.6619	1.13287
N	-3.78734	-1.57352	0.00524	N	2.14221	1.3111	2.54547	C	4.37112	6.05498	1.49762
N	-3.5538	0.53952	-0.02563	N	1.42619	3.31884	2.38216	C	6.26599	0.8117	0.00939
N	-3.73661	1.91889	-0.0352	N	1.27233	4.7009	2.40206	C	3.75318	1.03498	1.51974
H	-4.31187	2.1545	-0.84223	H	1.18419	4.99795	3.37201	N	5.96295	4.54103	0.45676
O	2.74805	3.26888	0.66121	O	-3.54634	4.49255	-1.98517	N	2.47754	1.02688	1.61654
O	1.61314	-2.00956	0.07964	O	-1.54823	-0.50184	-1.12247	O	2.8777	3.69756	2.17998
H	0.75457	-1.53789	0.0227	S	3.76342	3.13642	3.80505	O	7.1179	0.98778	-1.10999
S	-6.18713	-0.22184	0.04571	H	-3.21693	4.37843	-2.88347	N	0.02799	2.0505	2.70756
H	3.15546	3.03253	1.50166	H	2.6659	0.47822	2.75607	N	1.19711	-0.59953	-2.47332
H	-4.15035	-2.5119	0.02439	H	2.12975	5.11577	2.04101	C	6.32435	-3.24896	-0.77825
H	-4.2762	2.17042	0.79147	Zn	-0.01316	-0.00802	0.09726	C	5.50869	-2.43757	-1.55675
				O	1.50271	0.58275	-1.10546	C	4.14944	-2.30191	-1.17642
				C	2.4764	-0.00791	-1.70047	C	3.7383	-2.9724	-0.00643
				C	2.85888	-1.37109	-1.49535	C	4.64848	-3.77277	0.71154
				C	3.25965	0.75041	-2.65594	C	4.20498	-4.50487	1.94697
				C	3.99035	-1.87835	-2.20913	C	6.10256	-1.74117	-2.76266
				C	2.14441	-2.2542	-0.61601	C	3.22154	-1.47659	-1.94237

C	2.87552	2.17938	-2.91422	N	5.9109	-3.9022	0.3149
N	4.28589	0.24783	-3.3058	N	1.96444	-1.3997	-1.66573
C	4.64335	-1.03831	-3.08182	O	2.48558	-2.86295	0.50152
C	4.51816	-3.28192	-2.01946	O	7.49401	-1.50534	-2.51347
H	2.46705	-3.29527	-0.61389	N	-1.07002	-2.46029	-1.42915
N	1.13101	-1.92615	0.12555	H	2.3214	-1.03389	1.81219
H	2.94753	2.77454	-1.99835	H	7.30177	3.26236	-0.45586
H	1.83549	2.24954	-3.24642	H	5.10921	6.7653	1.12959
H	3.5358	2.59747	-3.67304	H	4.28654	6.19402	2.58346
H	5.50664	-1.39152	-3.63853	H	3.40204	6.30273	1.0493
H	5.41767	-3.40688	-2.63236	H	5.44064	0.13474	-0.23936
H	4.80975	-3.45745	-0.97998	H	6.81149	0.35383	0.85029
O	3.56418	-4.31426	-2.31102	H	4.32974	0.12011	1.68189
N	0.57701	-2.95136	0.89007	H	2.82521	4.60581	2.49764
H	3.22688	-4.14957	-3.19847	H	7.45008	0.11852	-1.38131
C	-0.54802	-2.60469	1.56067	H	-0.80143	2.64146	2.7003
H	0.65564	-3.91746	0.5865	H	0.79834	2.49191	2.20515
N	-0.96358	-1.37746	1.72646	H	1.67564	0.17171	-2.93286
N	-1.38032	-3.50234	2.17248	H	7.36766	-3.36589	-1.04196
N	-2.12818	-1.52101	2.46538	H	5.02806	-5.11969	2.30721
C	-2.4323	-2.79889	2.77531	H	3.33574	-5.13555	1.74291
N	-1.20088	-4.88003	2.10944	H	3.9069	-3.80938	2.73788
H	-2.6639	-0.71177	2.73097	H	5.6069	-0.78323	-2.95059
S	-3.6989	-3.44671	3.63613	H	5.98225	-2.36677	-3.65668
H	-1.08806	-5.23109	3.05858	H	3.61975	-0.90379	-2.78149
H	-2.05741	-5.28996	1.74079	H	1.92815	-2.35982	-0.12728
				H	7.91867	-1.27835	-3.34722
				H	-0.36337	-2.5292	-0.69808
				H	-0.86501	-3.08119	-2.20563

Table S8. The Cartesian coordinates of **L** (enol-thione), **ZnL₂** and **Hg₂L₂** calculated from Gaussian-09 at B3LYP computational level using IEF-PCM calculation (**DMSO as solvent**).

L (enol-thione)				ZnL₂			Hg₂L₂				
C	4.80547	0.48956	-0.15016	C	-4.67713	1.29266	-2.96325	Hg	-3.48257	2.29401	-0.61677
H	5.70724	1.09272	-0.21596	H	-5.53807	1.69471	-3.48958	S	-3.00967	1.48107	1.84359
C	3.56264	1.10067	-0.19737	C	-4.00777	2.06212	-2.03929	N	-0.18996	-1.16572	1.21983
C	2.41274	0.27559	-0.10527	C	-2.87912	1.49236	-1.36954	N	-1.50928	-0.76825	1.21819
C	2.61358	-1.1157	0.00292	C	-2.51691	0.14138	-1.66958	N	-0.3285	0.88352	2.01339
C	3.93311	-1.62828	0.04193	C	-3.3158	-0.53932	-2.66946	N	1.85155	-0.13992	1.95402
C	4.15178	-3.10917	0.17121	C	-2.95284	-1.95227	-3.02718	C	0.49204	-0.16477	1.73181
H	3.69898	-3.64707	-0.66702	H	-3.032	-2.60861	-2.15469	C	-1.59604	0.47863	1.66075

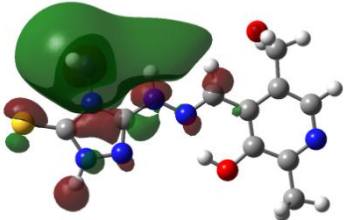
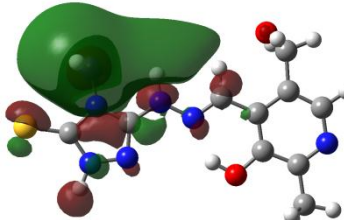
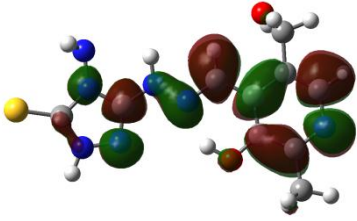
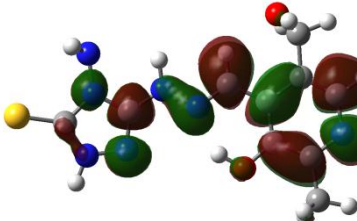
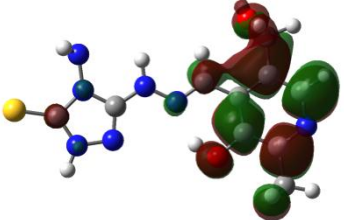
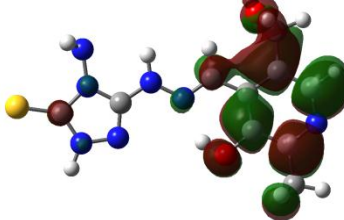
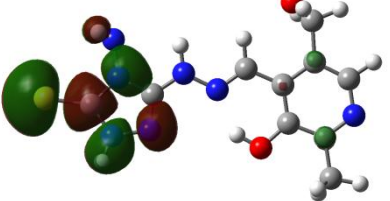
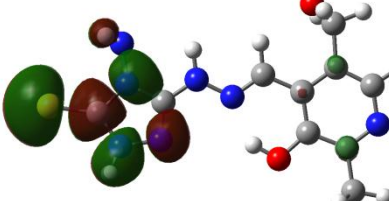
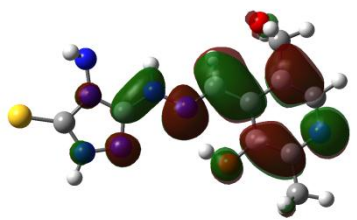
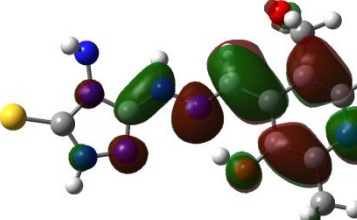
H	3.68253	-3.49823	1.07958	H	-1.91452	-2.01417	-3.3662	Hg	-3.23753	-2.38503	0.50966
H	5.22166	-3.31019	0.1976	H	-3.62049	-2.30723	-3.81131	N	-1.89617	0.91474	-1.93402
C	3.47638	2.59888	-0.37483	C	-4.51309	3.45719	-1.75166	S	-3.89505	-0.85423	-1.49513
H	4.49043	3.00587	-0.46151	H	-5.41667	3.6358	-2.345	Cl	-3.61941	-4.43447	1.81421
H	2.94794	2.85268	-1.29791	H	-4.79141	3.56768	-0.69969	C	-2.25552	-0.34165	-1.75448
C	1.07643	0.85669	-0.10899	C	-2.14615	2.30536	-0.43887	N	-0.53165	0.97868	-2.15014
H	0.99286	1.94358	-0.07816	H	-2.45269	3.34884	-0.3671	C	-0.09357	-0.24518	-2.10556
C	-2.31759	-0.07099	-0.0471	C	0.56969	2.47373	1.73025	N	-1.12747	-1.13252	-1.86223
C	-4.53472	-0.45105	0.00925	C	2.47358	2.56266	2.9263	Cl	-4.67995	4.1365	-1.74909
N	4.99348	-0.83306	-0.03051	N	-4.33844	0.02034	-3.27709	C	6.38558	3.3202	0.1174
N	0.03124	0.10363	-0.09873	N	-1.13325	1.91467	0.27221	C	5.70688	2.15018	0.44199
N	-1.18667	0.69062	-0.08416	N	-0.55655	2.87978	1.0958	C	4.49477	2.25159	1.15792
H	-1.30459	1.69997	-0.07711	H	-0.621	3.86424	0.85406	C	4.05185	3.54281	1.49424
N	-2.41502	-1.3674	-0.0289	N	0.96506	1.23167	1.81671	C	4.82186	4.6619	1.13287
N	-3.78734	-1.57352	0.00524	N	2.14221	1.3111	2.54547	C	4.37112	6.05498	1.49762
N	-3.5538	0.53952	-0.02563	N	1.42619	3.31884	2.38216	C	6.26599	0.8117	0.00939
N	-3.73661	1.91889	-0.0352	N	1.27233	4.7009	2.40206	C	3.75318	1.03498	1.51974
H	-4.31187	2.1545	-0.84223	H	1.18419	4.99795	3.37201	N	5.96295	4.54103	0.45676
O	2.74805	3.26888	0.66121	O	-3.54634	4.49255	-1.98517	N	2.47754	1.02688	1.61654
O	1.61314	-2.00956	0.07964	O	-1.54823	-0.50184	-1.12247	O	2.8777	3.69756	2.17998
H	0.75457	-1.53789	0.0227	S	3.76342	3.13642	3.80505	O	7.1179	0.98778	-1.10999
S	-6.18713	-0.22184	0.04571	H	-3.21693	4.37843	-2.88347	N	0.02799	2.0505	2.70756
H	3.15546	3.03253	1.50166	H	2.6659	0.47822	2.75607	N	1.19711	-0.59953	-2.47332
H	-4.15035	-2.5119	0.02439	H	2.12975	5.11577	2.04101	C	6.32435	-3.24896	-0.77825
H	-4.2762	2.17042	0.79147	Zn	-0.01316	-0.00802	0.09726	C	5.50869	-2.43757	-1.55675
				O	1.50271	0.58275	-1.10546	C	4.14944	-2.30191	-1.17642
				C	2.4764	-0.00791	-1.70047	C	3.7383	-2.9724	-0.00643
				C	2.85888	-1.37109	-1.49535	C	4.64848	-3.77277	0.71154
				C	3.25965	0.75041	-2.65594	C	4.20498	-4.50487	1.94697
				C	3.99035	-1.87835	-2.20913	C	6.10256	-1.74117	-2.76266
				C	2.14441	-2.2542	-0.61601	C	3.22154	-1.47659	-1.94237
				C	2.87552	2.17938	-2.91422	N	5.9109	-3.9022	0.3149
				N	4.28589	0.24783	-3.3058	N	1.96444	-1.3997	-1.66573
				C	4.64335	-1.03831	-3.08182	O	2.48558	-2.86295	0.50152
				C	4.51816	-3.28192	-2.01946	O	7.49401	-1.50534	-2.51347
				H	2.46705	-3.29527	-0.61389	N	-1.07002	-2.46029	-1.42915
				N	1.13101	-1.92615	0.12555	H	2.3214	-1.03389	1.81219
				H	2.94753	2.77454	-1.99835	H	7.30177	3.26236	-0.45586
				H	1.83549	2.24954	-3.24642	H	5.10921	6.7653	1.12959
				H	3.5358	2.59747	-3.67304	H	4.28654	6.19402	2.58346
				H	5.50664	-1.39152	-3.63853	H	3.40204	6.30273	1.0493
				H	5.41767	-3.40688	-2.63236	H	5.44064	0.13474	-0.23936
				H	4.80975	-3.45745	-0.97998	H	6.81149	0.35383	0.85029

O	3.56418	-4.31426	-2.31102	H	4.32974	0.12011	1.68189
N	0.57701	-2.95136	0.89007	H	2.82521	4.60581	2.49764
H	3.22688	-4.14957	-3.19847	H	7.45008	0.11852	-1.38131
C	-0.54802	-2.60469	1.56067	H	-0.80143	2.64146	2.7003
H	0.65564	-3.91746	0.5865	H	0.79834	2.49191	2.20515
N	-0.96358	-1.37746	1.72646	H	1.67564	0.17171	-2.93286
N	-1.38032	-3.50234	2.17248	H	7.36766	-3.36589	-1.04196
N	-2.12818	-1.52101	2.46538	H	5.02806	-5.11969	2.30721
C	-2.4323	-2.79889	2.77531	H	3.33574	-5.13555	1.74291
N	-1.20088	-4.88003	2.10944	H	3.9069	-3.80938	2.73788
H	-2.6639	-0.71177	2.73097	H	5.6069	-0.78323	-2.95059
S	-3.6989	-3.44671	3.63613	H	5.98225	-2.36677	-3.65668
H	-1.08806	-5.23109	3.05858	H	3.61975	-0.90379	-2.78149
H	-2.05741	-5.28996	1.74079	H	1.92815	-2.35982	-0.12728
				H	7.91867	-1.27835	-3.34722
				H	-0.36337	-2.5292	-0.69808
				H	-0.86501	-3.08119	-2.20563

Table S9. Major UV-Vis electronic transitions and corresponding orbital contributions for **L**, **ZnL₂**, and **Hg₂L₂**.

	Solvent system	Experimental wavelength (nm)	Theoretical wavelength (nm)	Oscillator strength (f)	Major contributing transition	Character
L	Water	257	280.6703	0.5393	HOMO-3→LUMO (88%) HOMO-4→LUMO (4%)	$\pi \rightarrow \pi^*$
		336	359.1221	0.3750	HOMO→LUMO (99%)	
	DMSO	272	281.2306	0.5484	HOMO-3→LUMO (88%) HOMO-4→LUMO (4%)	
		336	360.1549	0.3861	HOMO→LUMO (99%)	
ZnL₂	Water	247	247.5112	0.3061	HOMO-2→LUMO+2 (75%) HOMO-13→LUMO+1 (2%) HOMO-12→LUMO (2%) HOMO-11→LUMO+1 (2%) HOMO-10→LUMO (3%) HOMO-3→LUMO+3 (4%) HOMO→LUMO+4 (5%)	$\pi \rightarrow \pi^*$
		400	380.9362	0.3292	HOMO-1→LUMO+1 (60%) HOMO→LUMO (35%)	ILCT
	DMSO	271	280.9247	0.4026	HOMO-9→LUMO (54%) HOMO-8→LUMO+1 (26%) HOMO→LUMO+2 (10%) HOMO-1→L+3 (4%)	$\pi \rightarrow \pi^*$
		407	382.0985	0.3403	HOMO-1→LUMO+1 (61%) HOMO→LUMO (34%)	ILCT + LMCT
Hg₂L₂	Water	362	363.0657	0.1866	HOMO-1→LUMO (93%) HOMO→LUMO (5%)	ILCT
			336.2807	0.3309	HOMO→LUMO+1 (85%) HOMO-1→LUMO+1 (4%) HOMO→LUMO+2 (8%)	
	DMSO	366	363.2359	0.1977	HOMO-1→LUMO (93%) HOMO→LUMO (4%)	
			336.6093	0.3397	HOMO→LUMO+1 (83%) HOMO→LUMO+2 (10%) HOMO-1→LUMO+1 (3%)	

Table S10. Selected Frontier molecular orbitals HOMO-LUMO diagram of probe (**L**) in water and DMSO medium.

Molecular orbital state	L (Enol-thione form)			
	Water medium	E (eV)	DMSO medium	E (eV)
LUMO+4		0.9319		0.9235
LUMO+3		0.3662		0.3651
LUMO+2		-0.4430		-0.4432
LUMO+1		-0.5382		-0.5371
LUMO		-2.0623		-2.0637

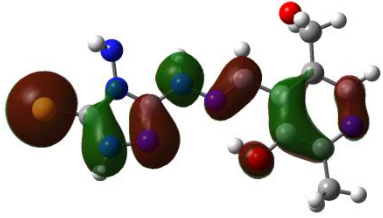
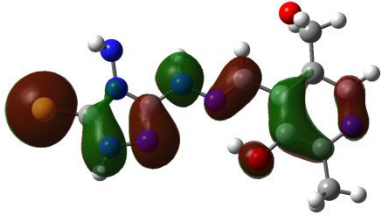
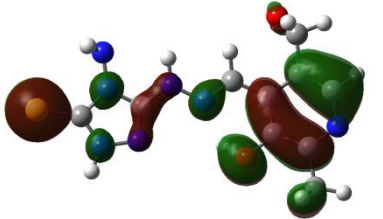
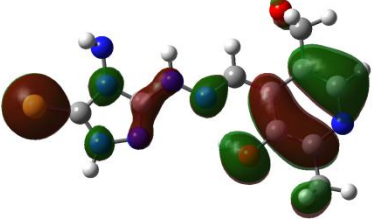
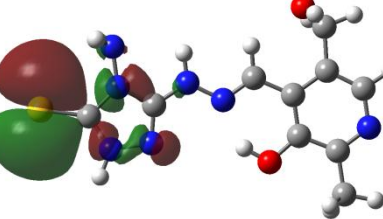
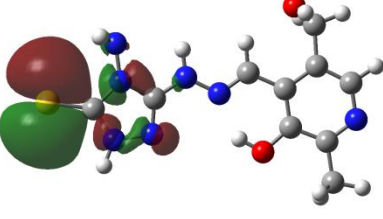
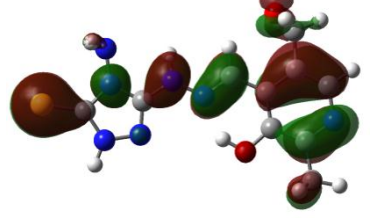
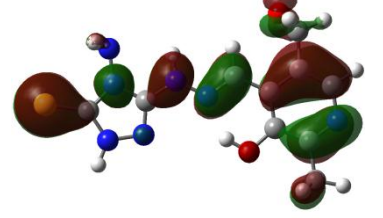
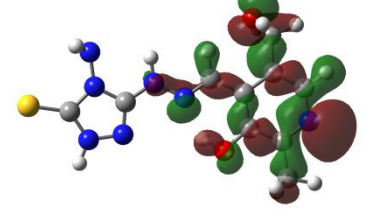
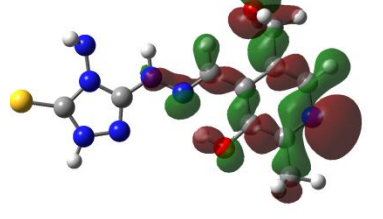
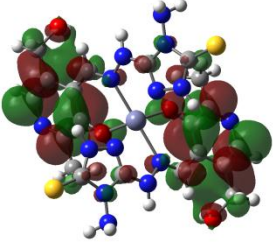
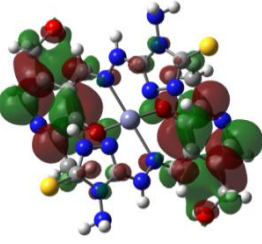
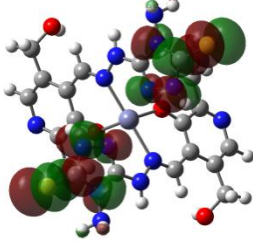
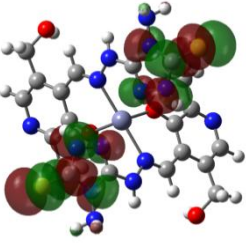
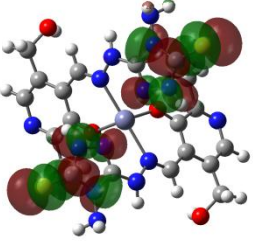
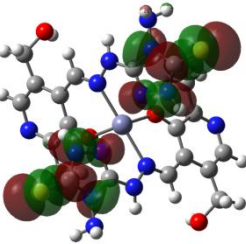
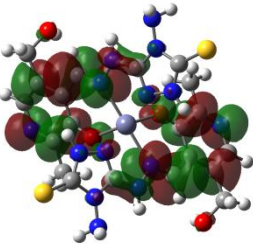
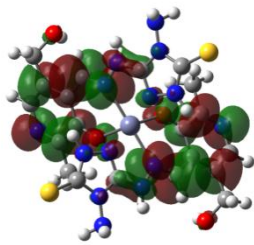
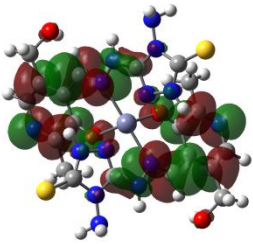
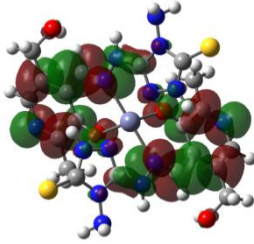
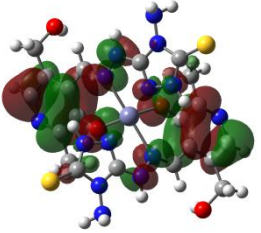
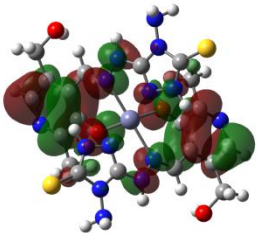
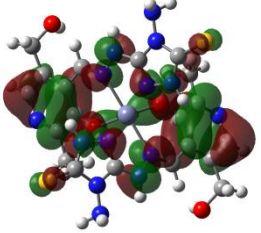
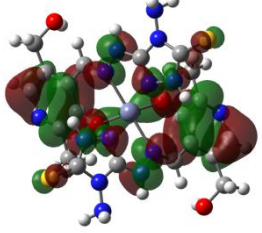
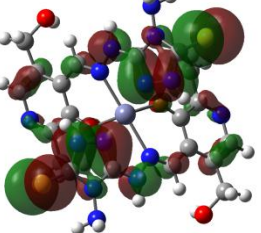
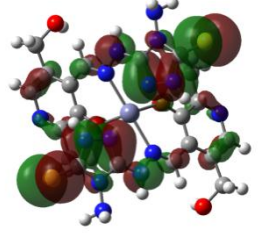
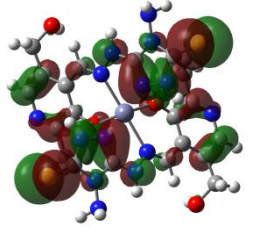
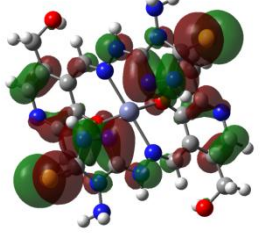
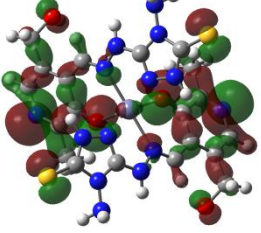
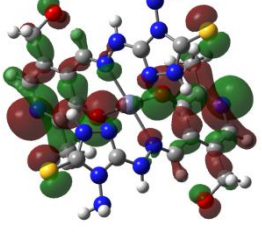
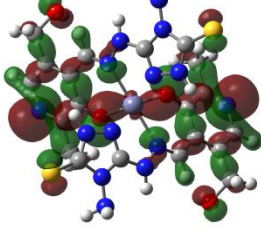
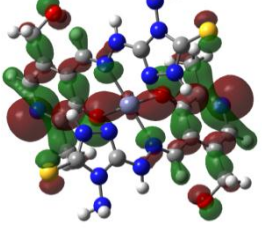
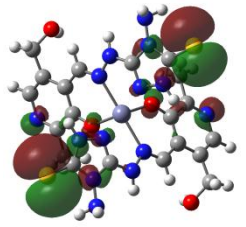
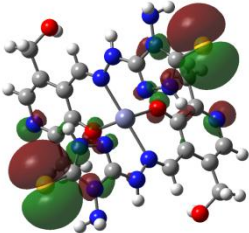
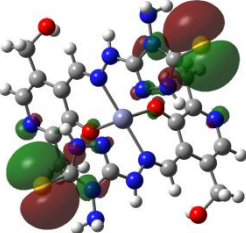
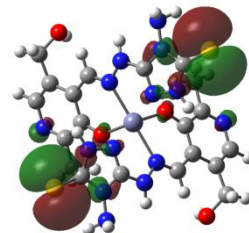
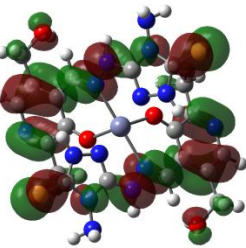
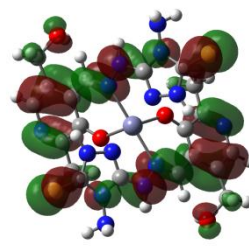
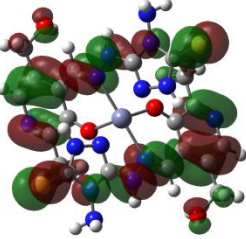
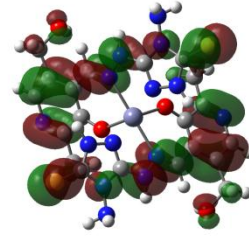
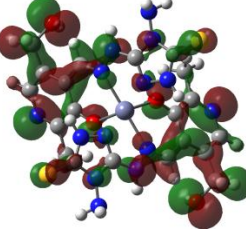
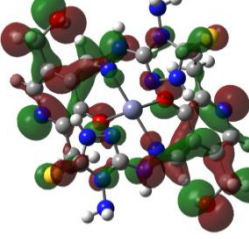
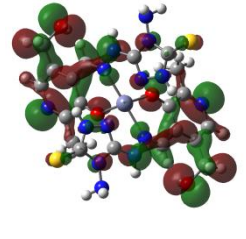
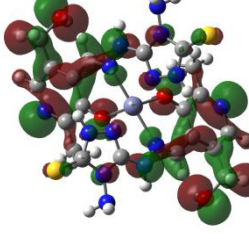
HOMO		-5.9443		-5.9435
HOMO-1		-6.4518		-6.4507
HOMO-2		-6.5927		-6.5884
HOMO-3		-6.9394		-6.9399
HOMO-4		-7.2142		-7.2121

Table S11. Selected Frontier molecular orbitals HOMO-LUMO diagram of zinc(II) complex (ZnL_2) in water and DMSO medium.

Molecular orbital state	ZnL_2			
	Water medium	E (eV)	DMSO medium	E (eV)
LUMO+4		-0.1150		-0.1099
LUMO+3		-0.7257		-0.7270
LUMO+2		-0.7379		-0.7396
LUMO+1		-2.0139		-2.0139
LUMO		-2.0509		-2.0506

HOMO		-5.6855		-5.6836
HOMO-1		-5.6904		-5.6888
HOMO-2		-6.2101		-6.2104
HOMO-3		-6.3018		-6.3016
HOMO-4		-6.5663		-6.5625
HOMO-5		-6.6305		-6.6267

HOMO-6		-6.6986		-6.6967
HOMO-7		-6.7018		-6.6999
HOMO-8		-6.9674		-6.9674
HOMO-9		-6.9764		-6.9761
HOMO-10		-7.7574		-7.7576
HOMO-11		-7.7843		-7.7843

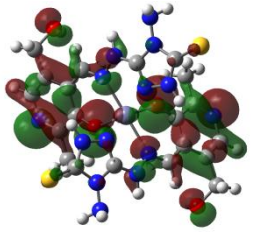
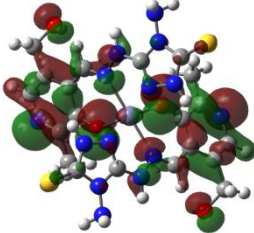
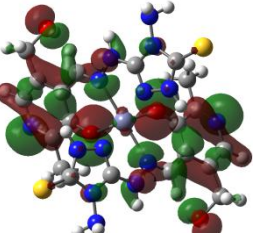
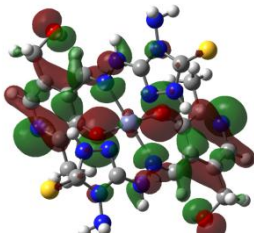
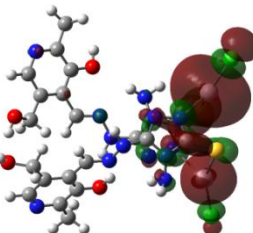
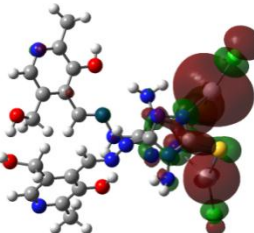
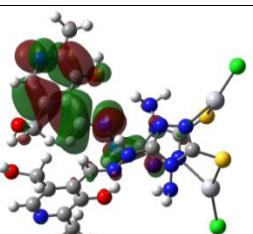
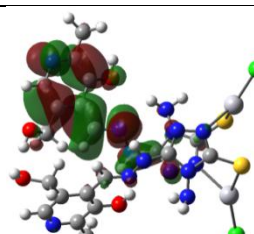
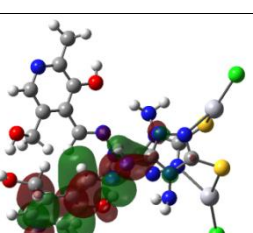
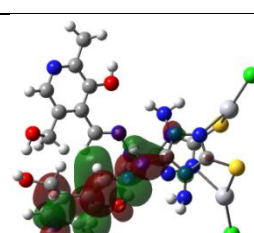
HOMO-12		-7.9620		-7.9593
HOMO-13		-7.9949		-7.9927

Table S12. Selected Frontier molecular orbitals HOMO-LUMO diagram of mercury(II) complex (Hg_2L_2) in water and DMSO medium.

Molecular orbital state	Hg_2L_2			
	Water medium	E (eV)	DMSO medium	E (eV)
LUMO+2		-1.5017		-1.5298
LUMO+1		-1.7910		-1.7962
LUMO		-2.1739		-2.1845

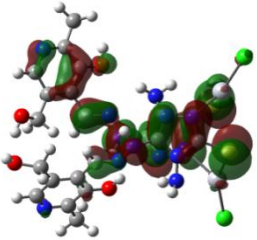
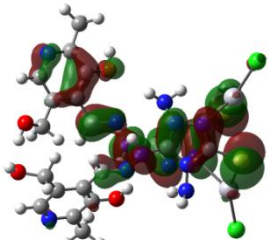
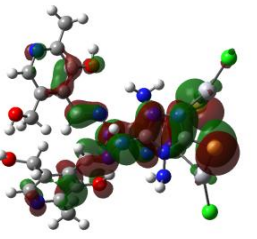
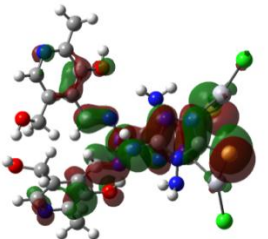
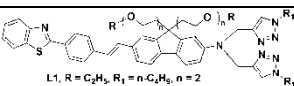
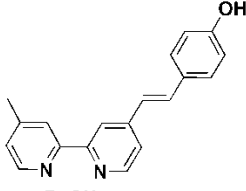
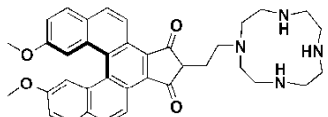
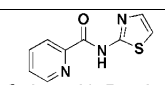
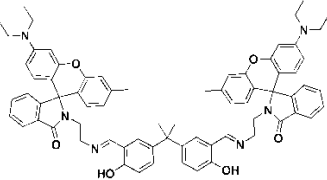
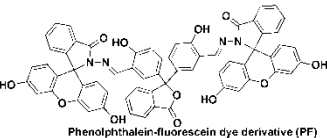
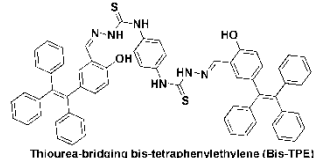
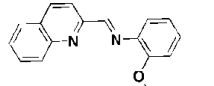
HOMO		-5.9682		-5.9802
HOMO-1		-6.0643		-6.0771

Table S13. Comparison with recent literature results.

Zn ²⁺ and Hg ²⁺ sensors	Sensing Medium	LOD	Stoichiometry	Application	Sensing mechanism	Ref.
 L1, R = C ₆ H ₅ , R ₁ = n-C ₁₂ H ₂₅ , n = 2 L2, R = C ₆ H ₅ , R ₁ = n-C ₁₁ H ₂₃ SH, n = 2 L3, R = CH ₃ , R ₁ = n-C ₁₁ H ₂₃ SH, n = 6-10 Hydrophilic bis(1,2,3-triazolyl)fluorene-based derivatives containing a 1,2,3-triazole-based recognition moiety	Ethanol	-	1:2 (L:Zn ²⁺) and 1:3 (L:Hg ²⁺)	Two-Photon based metal ion sensing.	ICT	[11]
Fluorescence peptide-based sensor (Dansyl-His-Thr-Glu-His-Trp-NH ₂ , D-P5)	Aqueous medium	For Zn ²⁺ , 37.8 nM; For Hg ²⁺ , 59.4 nM	1:1 (L:Zn ²⁺) and L:Hg ²⁺)	This sensor also used for Cu ²⁺ ion. Real water sample application	-	[12]
 BsOH	Methanol	For Zn ²⁺ , 900 nM For Hg ²⁺ , 290 nM	-	This sensor also used for Cu ²⁺ ion. Real water sample application.	Inhibition of PET	[13]
 Helical imide as fluorophore and a cyclen moiety as ionophore	HEPES (10 mM, pH = 7.2)	-	1:1 (L:Zn ²⁺ and L:Hg ²⁺)	This sensor also used for Cd ²⁺ ion. Distinguish three cations with the help of cysteine as an auxiliary reagent.	Inhibition of PET	[14]

Fluorescent peptide dansyl-HPHGHW-NH ₂ (dH3w)	MOPS (20 mM buffer, pH 7)	-	2:1 (Peptide:Zn ²⁺) 1:1 and 1:2, (Peptide/Hg ²⁺)	More efficient fluorescence peptidyl probes for Zn ²⁺ and Hg ²⁺ with unusual complexation mode	-	[15]
 Carboxamide-Based probe	ACN	-	1:1 (L:Zn ²⁺ and L:Hg ²⁺)	This sensor also used for Cd ²⁺ ion. The probe has low cytotoxicity with PC12 cells	CHEF	[16]
 Bisphenol A-rhodamine	ACN-H ₂ O (v/v=8/2, 5 mM, HEPES, pH 7.0)	For Zn ²⁺ , 2210 nM For Hg ²⁺ , 2160 nM	1:2 (L:Zn ²⁺ and L:Hg ²⁺)	Intracellular imaging in live cells (PC-3)	ESIPT and FRET	[17]
 Phenolphthalein-fluorescein dye derivative (PF)	EtOH-H ₂ O (v/v = 8/2, 5 mM, HEPES, pH 7.0)	For Zn ²⁺ , 540 nM For Hg ²⁺ , 1160 nM	1:2 (L:Zn ²⁺ and L:Hg ²⁺)	Determination of Zn ²⁺ and Hg ²⁺ in real water samples	Inhibition of ICT, FRET and -C=N isomerization	[18]
 Thiourea-bridging bis-tetraphenylethylene (Bis-TPE)	H ₂ O-THF solution (90 % of H ₂ O)	For Zn ²⁺ , 82.2 nM For Hg ²⁺ , 34.3 nM	1:1 (L:Zn ²⁺ and L:Hg ²⁺)	First examples for simultaneous detection of group IIB elements (Zn ²⁺ , Cd ²⁺ and Hg ²⁺). Test strips and cell-imaging applications.	AIE	[19]
 ((E)-2-methoxy-N-((quinolin-2-yl)methylene)aniline) (MQA)	DMSO-H ₂ O solution (1/99 v/v)	For Zn ²⁺ , 11 nM For Hg ²⁺ , 40 nM	1:1 (L:Zn ²⁺ and L:Hg ²⁺)	Reversible sensing with distinct emission response towards Zn ²⁺ and Hg ²⁺ .	ICT and CHEF	[20]

<p>Rhodamine 6G condensed isophorone moiety (RHI)</p>	EtOH/H ₂ O (8/2, v/v)	For Zn ²⁺ , 82.2 nM For Hg ²⁺ , 1130 nM	2:1 (L:Zn ²⁺) and 1:1 (L:Hg ²⁺)	Real water samples and bio-imaging in DDL-1 cells.	CHEF	[21]
<p>N-(naphthalen-1-yl)-2-(thiophene-2-carbonyl)hydrazine-1-carbothioamide (NTHC)</p>	Aqueous DMSO (For Zn ²⁺) and Bis-tris buffer (For Hg ²⁺)	For Zn ²⁺ , 3170 nM For Hg ²⁺ , 4920 nM	1:1 (L:Zn ²⁺ and L:Hg ²⁺)	Bioimaging in Zebrafish (air bladder and eyes) and interestingly desulfurization reaction of thiourea to urea in case of Hg ²⁺ detection.	CHEF	[22]
<p>Thiocarbonohydrazone locked salicylidene based probe</p>	DMSO-HEPES buffer (9:1 v/v, pH 7.4)	For Zn ²⁺ , 99 nM For Hg ²⁺ , 14 nM	1:2 (L:Zn ²⁺) and 1:4 (L:Hg ²⁺)	Logic gate applications. Also applied to detect trace amount of S ²⁻ ions.	CHEF and inhibition of intramolecular PET	[23]
<p>Pyridoxal-AHMT</p>	HEPES buffered (pH = 8.0) (DMSO:water (1:1, v/v))	For Zn ²⁺ , 522.50 nM For Hg ²⁺ , 1059.20 nM	2:1 (L:Zn ²⁺) and 1:1 (L:Hg ²⁺)	Solid and solution state sensing, cell imaging application	CHEF (for Zn ²⁺) and CHEQ (for Hg ²⁺) and ESIPT suppression	This work

Reference

- [1] P. Kubelka, and F. Munk, *Z. Techn. Phys.*, 1931, **12**, 593 -601.
- [2] P. Makuła, M. Pacia, and W. Macyk, *J. Phys. Chem. Lett.*, 2018, **9**, 6814–6817.
- [3] Z. D. Hill, and M. Patrick, *J. Chem. Educ.*, 1986, **63**, 162-167.
- [4] G. S. Forbes, L. J. Heidt, and C. G. Boissonas, *J. Am. Chem. Soc.*, 1932, **54**, 960–973.
- [5] M. A. Spackman, and D. Jayatilaka, *CrystEngComm*, 2009, **11**, 19–32.
- [6] H. A. Benesi, and J. H. Hildebrand, *J. Am. Chem. Soc.*, 1949, **71**, 2703-2707.
- [7] S. Guo, C. Fan, G. Liu, and S. Pu, *RSC Adv.*, 2018, **8**, 39854–39864.
- [8] P. Purushothaman, and S. Karpagam, *ACS Omega*, 2022, **7**, 41361–41369.
- [9] M. A. Spackman, and J. J. McKinnon, *CrystEngComm*, 2002, **4**, 378-392.
- [10] H. Ferjani, H. Chebbi, A. Guesmi, O. S. AlRuqi, and S. A. Al-Hussain, *Crystals*, 2019, **9**, 2-10.
- [11] D. M. Nguyen, A. Frazer, L. Rodriguez, and K. D. Belfield, *Chem. Mater.*, 2010, **22**, 3472–3481.
- [12] L. Zhang, S. Yu, L. Gao, W. Meng, C. Fu, and L. Li, *Spectrosc. Lett.*, 2022, **55**, 488-499.
- [13] S. C. L. Pinheiro, I. M. Raimundo Jr, M. C. Moreno-Bondi, and G. Orellana, *Anal. Bioanal. Chem.*, 2010, **398**, 3127–3138.
- [14] M. Li, H.-Y. Lu, R.-L. Liu, J.-D. Chen, and C.-F. Chen, *J. Org. Chem.*, 2012, **77**, 3670–3673.
- [15] M. Siepi, R. Oliva, F. Battista, L. Petraccone, P. D. Vecchio, V. Izzo, F. D. Piaz, R. Isticato, E. Notomista, and G. Donadio, *Sensors*, 2020, **20**, 1-16.

- [16] M. Kiani, M. Bagherzadeh, S. Meghdadi, N. Rabiee, A. Abbasi, K. Shenk-Joß, M. Tahriri, L. Tayebi, and T. J. Webster, *New J. Chem.*, 2020, **44**, 11841-11852.
- [17] S. Erdemir, M. Yuksekogul, S. Karakurt, and O. Kocyigit, *Sens. Actuators B Chem.*, 2017, **241**, 230-238.
- [18] S. Erdemir, and O. Kocyigit, *Dyes Pigm.*, 2017, **145**, 72-79.
- [19] S. Jiang, S. Chen, Z. Wang, H. Guoa, and F. Yang, *Sens. Actuators B Chem.*, 2020, **308**, 127734.
- [20] Y. Dong, R. Fan, W. Chen, P. Wang, and Y. Yang, *Dalton Trans.*, 2017, **46**, 6769-6775.
- [21] S. Erdemir, and S. Malkondu, *J. Mol. Liq.*, 2021, **326**, 115279.
- [22] H. Kim, M. Lee, J. J. Lee, E. K. Min, K. -T. Kim, and C. Kim, *J. Photochem. Photobiol. A: Chem.*, 2022, **428**, 113882.
- [23] S. K. Padhan, J. Palei, P. Rana, N. Murmu, and S. N. Sahu, *Spectrochim. Acta A Mol.*, 2019, **208**, 271-284.